Chemical Geology
Manuscript Draft

Manuscript Number: CHEMGE9789

Title: Hydrological versus volcanic processes affecting fluid circulation at Mt Etna volcano: inferences from 10 years of observations at the volcanic aquifer

Article Type: Research paper

Hydrological versus volcanic processes affecting fluid circulation at Mt Etna volcano: inferences from 10 years of observations at the volcanic aquifer

Manfredi Longo[1], Cinzia Federico[1,*], Walter D'Alessandro[1], Sergio Bellomo[1], Pietro Bonfanti[2], Lorenzo Brusca[1]

[1] Istituto Nazionale di Geofisica e Vulcanologia - Sezione di Palermo, Via Ugo La Malfa 153, 90146 Palermo, Italy

[2] Istituto Nazionale di Geofisica e Vulcanologia - Osservatorio Etneo, Piazza Roma 2, 95123 Catania, Italy

* Corresponding author: cinzia.federico@ingv.it

Abstract

The time series of geochemical data available for the network of wells and drainage galleries at Mt Etna has been analyzed to identify the changes in water chemistry related to the input of volcanic CO_2 and those related to hydrogeological dynamics. The dynamics of hydrological systems is mainly affected by changes in the rainfall, since this influences the yields of both springs and drainage galleries and the water-table height of unconfined aquifers. In addition, the characteristics of hydrological systems can change with the fluid pressure. These mechanisms are probably enhanced by changes in the crustal strain, which can cause inter-basin transfer of water. The changes in water circulation are paralleled by variations in physicochemical characteristics of groundwater, since water transfer probably occurs among water bodies with different temperatures and compositions.

Based on the above mechanisms, the contribution of different water types has been estimated according to their chemical composition: it has been assumed that water circulating in the volcanic pile has a typical HCO_3-rich composition, whereas Cl, SO_4, and NO_3 could be contributed by rainfall, anthropogenic pollution, and sedimentary fluids rich in Na and Cl. In some cases the SO_4 enrichment is related to the dissolution of SO_4-bearing alteration minerals. We hypothesize a binary mixing between the HCO_3-rich volcanic end member and an end member polluted with Cl, SO_4, and NO_3 related to water circulation at shallow levels. These two end members are identified by their $HCO_3/(Cl+SO_4+NO_3)$ ratio and Cl, SO_4, and NO_3 contents measured at each sampling site. The extent of mixing between these different water types changes over time, probably due to changes in their circulation patterns, with water being transferred from/to water bodies with different compositions. Once the proportion of the HCO_3 content related to the binary mixing is determined, we can compute the amount of HCO_3 related to the variable input of CO_2 over time into the aquifer. The obtained time trends are synchronous in the two sectors of the volcano where the maximal CO_2 degassing occurs, namely the Paterno-Belpasso area on the southwestern flank and the Zafferana-S. Venerina area on the eastern flank. This provides evidence for a common deep mechanism underlying the CO_2 variations that is related to the dynamics of the volcano.

Introduction

Stratovolcanoes are extensively permeated by both volcanic fluids ascending from depth through rifts or faults, and meteoric waters infiltrating through permeable lavas and pyroclastics. Both shallow and deep fluids can interact widely to give rise to hydrothermal systems under appropriate structural and geological conditions. Shallow groundwaters are affected only slightly by magmatic-hydrothermal fluids, mainly showing evidence of CO_2-driven water–rock interactions. Fluid circulation in a volcanic environment has received increasing interest from scientists for various reasons. First, temporal monitoring of the composition and mass rate of volcanic fluids emitted from fumaroles, mofettes, thermal springs, and wells is routinely performed worldwide for volcanic surveillance purposes. The chemical and isotope compositions of high-temperature gases, as well as the chemistry and flux of plume gases provide insights into magma degassing and the dynamics of plumbing systems (Oppenheimer et al., 2003, Aiuppa et al., 2009; Aiuppa et al., 2010; Caracausi et al., 2003b; Rizzo et al., 2006). Measurements on mofettes, thermal springs and wells, and CO_2-rich groundwaters reveal the pattern of ascent of volcanic and hydrothermal fluids, even kilometers away from the vents, while the eventual changes in composition and mass rate help when tracking the evolution of magmatic and hydrothermal systems (Chiodini et al., 2002, 2010; Lowenstern et al., 2006; Paonita et al., 2012). Second, fluids can dramatically affect the stability of volcanic edifices by changing rock geotechnical characteristics through hydrothermal alteration and/or fluid pressurization. Gas overpressure has been proposed as an instability mechanism underlying failures of domes and flanks (Day, 1996; Voight and Elsworth, 2000; Reid, 2004; Thomas et al., 2004). Moreover, fluid pressurization within hydrothermal systems regardless of whether or not it is eventually related to magma degassing episodes is considered the process driving periodic deformation in restless calderas (Dzurisin et al., 1999; Battaglia et al., 2006; Gottsmann et al., 2007). Finally, crustal and fault permeabilities are critically controlled by fluids; self-sealing phenomena associated with mineral deposition from supersaturated aqueous solutions reduce rock permeability, whereas fluid overpressure that exceeds the rock strength induces microfracturing and increases the permeability (Rojstazczer et al., 2008; Capasso et al., 2014; Claesson et al., 2007). Fluid-induced rock failure gives rise to typical seismicity, called "hydroseismicity", as observed worldwide in both volcanic and tectonic settings (Christiansen et al., 2005; Ventura and Vilardo, 2005; Gudmundsson et al., 2001).

A reciprocal role can be hypothesized for the interaction between fluids and volcanic structures. Fluid overpressure could affect ground deformation and flank instability at volcanoes in the same manner as volcano deformation related to magma movement or tectonic strain can change the fluid pressure and modify fluid circulation (both of water and gases) within the volcanic edifice. Newhall et al. (2001) reported on various case studies of the effects of volcanic activity on the flow rates of springs and wells. Changes in water circulation (variations of spring outflow or pressure level in wells) can be induced by changes in crustal strain related to volcanic activity or earthquakes (Shibata and Akita, 2001; Hurwitz and Johnston, 2003; Koizumi et al., 2004; Niwa et al., 2012). Volcanoes are typically located in tectonically active areas, and it is challenging to fully understand the effects of volcanic activity, tectonic activity, or their combination on fluid circulation, as well as on their physicochemical features. Mt Etna is suitable for a case study due to the high frequency of its eruptions (Allard et al., 2006 and references therein), the existence of the well-developed INGV observation system (www.ingv.it), and the occurrence of significant seismic and deformation activity (Azzaro et al., 2013; Bruno et al., 2012 and references therein).

In this paper we propose an interpretative model of fluid circulation at Mt Etna that benefits from a huge amount of data collected during 1 decade of geochemical observations. Here we discuss the major-ion compositions of water samples collected from 2005 to 2015 from a network of selected wells, springs, and drainage galleries located on the lower flanks of the volcano. Geochemical data on the groundwater composition are evaluated to ascertain based on the observed variations the effects of the rainfall and of mixing between water circulating in different water bodies. The filtered results are interpreted in the context of multidisciplinary observations made during the same time span, which provides new insights into the effects of volcanic activity on water circulation and chemistry.

Geological setting

Mt Etna is a large stratovolcano located on the eastern coast of Sicily (latitude 37°30' to 37°55' North and longitude 14°47' to 15°15' East) covering an area of about 1,200 km^2 (Figure 1a). Etnean volcanism began at 0.5 Ma due to the breaking up of the African plate margin during its collision with the European continental block that began in the Upper Miocene (Barberi et al., 1974).

On the wide scale, the northeast–southwest and the northwest–southeast fault systems separate the Maghrebian-Appenninic chain to the north, which is part of the Euroasian plate, and the Hyblean platform to the south, which belongs to the African plate (Lentini, 1982). In such a regional context,

Mt Etna volcano has been built upon the tensional faults that cut through the continental crust where it is about 20 km thick (Chester et al., 1985), just at the intersection of the following three regional-scale fault systems:

1. The Tindari-Giardini system and the connected Maltese fault escarpment, both oriented northnorthwest–southsoutheast and elongated discontinuously from the Aeolian Islands to the island of Malta (Carbone et al., 1987).
2. The Comiso-Etna system and its inferred prolongation—the Messina-Capo Vaticano system trending northeast–southwest (Lo Giudice et al., 1982; Bousquet et al., 1988).
3. The Monte Kumeta-Alcantara system, oriented east–west, which runs through central Sicily and bounds the northern side of Mt Etna (Ghisetti and Vezzani, 1984).

Both the Maltese fault escarpment and the Comiso, Etna, and Messina systems appear to guide the ascent of Etnean magmas from depth, since most of the tectonic structures and eruptive fissures in the area of Mt Etna follow either of these two structural directions (Chester et al., 1985; Rasà et al., 1995). The magmas that erupt arise from a mantle diapir whose top lies at the base of the continental crust, whose shallowest portion is about 16 km deep (Hirn et al., 1997). The first erupted lavas were tholeiitic basalts, but most of the edifice formed through eruptions of alkali basalts and hawaiites (trachybasalts) with a relatively constant composition (Romano, 1982; Joron and Treuil, 1984; Chester et al., 1985; Tanguy et al., 1997). The present-day activity at Mt Etna is characterized by frequent summit and lateral eruptions (Tanguy et al., 1997) as well as large emissions of magmatic volatiles from the summit craters and the upper flanks, the latter as diffuse soil emanations (Allard et al., 1991, 1997). These emissions result from open-conduit degassing of alkali basalt and hawaiite magma (D'Alessandro et al., 1997a; Hirn et al., 1997).

The volcanic complex formed over Miocene flysch sediments (rising to an elevation of about 1300 m a.s.l.) to the northwest and clayey Pleistocene formations to the southeast, both belonging to the Maghrebian-Appenninic chain and overlying 10-km-thick carbonate sequences. Moreover, the presence of evaporitic rocks (gypsum, limestone, and sometimes S) deposited on top of the sedimentary sequence beneath the lavas on the southern flank of Mt Etna has also been hypothesized (Lentini, 1982).

Hydrogeology and hydrogeochemistry

As is commonly observed in strato volcanoes, Mt Etna is characterized by fissured and highly permeable lavas interbedded with discontinuous layers of low-permeability pyroclastics. The overall volcanic edifice can be considered as a highly porous medium, with a permeability

coefficient varying from 10^{-5} to 10^{-7} cm/s (Ferrara, 1975; Schilirò, 1988) depending on both the lithology and the volcano tectonic structures. The volcanic edifice lies on an impermeable sedimentary substratum whose permeability coefficients range from 10^{-7} to 10^{-13} cm/s (Schilirò, 1988).

The high permeability of volcanic rocks at Mt Etna is reflected by an infiltration coefficient for rainfall of about 75% and a runoff coefficient of about 5% (Ferrara, 1975). These features, together with the existence of an impermeable substratum, make Mt Etna an important groundwater reservoir, with about 7×10^{8} m^3 of water available annually. Indeed, basal springs, mostly located along the coastline, exhibit significant flow rates of up to 1000 l/s (Ogniben, 1966; Ferrara, 1975).

Water circulation at depth is confined by the sedimentary impermeable basement whose morphology controls the flow pathways of groundwater. Because the basement of Mt Etna reaches its highest elevation (about 1,300 m a.s.l.) a few kilometers northwest of the volcano summit and it generally dips to the southeast, groundwaters tend to flow and accumulate in the southern and eastern flanks of the volcanic edifice, and so this is where most of the springs and water wells are located (Ogniben, 1966; Branca and Ferrara, 2013).

Both geological and geophysical data on the morphology of the sedimentary basement have identified three major hydro geological basins bounded by hydrogeological divides (Figure 1):

1. One feeding the Alcantara River that lies in the northern sector of the volcano.
2. One feeding the Simeto River that lies on the south-western flank.
3. One that discharges into the Ionian Sea and lies on the eastern flank.

Data on the tritium content in both rainfall and groundwater (D'Alessandro et al., 2001), together with the estimated Darcy's velocity (Ferrara, 1975), indicate quite short residence times of a few years for Etnean groundwater. This excludes the saline waters circulating on the lower south-western slopes, which have longer and deeper flow pathways and an associated longer residence time in the aquifer (>50 years).

The existence of an impermeable basement beneath the volcanics of Mt Etna prevents its groundwaters from reaching considerable depths and thus results in the temperature of Etnean groundwaters generally being lower than 25°C (Aiuppa et al., 2003). Fluids from the underlying sedimentary basement locally ascend along the southern flank of the volcano and are emitted significantly from the mud volcanoes known as "Salinelle di Paternò." The features of waters discharged in this area are typical of hydrocarbon reservoirs and include a gas phase rich in CO_2 and CH_4. Geothermometric calculations based on both the water and gas chemistries for emissions in the Salinelle area yield estimated temperatures in the range of 100–150°C for their last equilibration (Chiodini et al., 1996).

The chemical and isotope compositions of the Etnean groundwaters have been studied widely (Anzà et al., 1989; Allard et al., 1997; Dall'Aglio et al., 1994; Giammanco et al., 1996, 1998; Aiuppa et al., 2000, 2002, 2003; Brusca et al., 2001). Data on water-stable isotopes indicate that the origin of Etnean groundwater is mainly meteoric, while the lack of any oxygen shift excludes high-temperature water–rock exchange processes. All authors agree about the fundamental role played by CO_2 dissolved in the aquifers in driving water–rock interactions and leading to the typical composition ranging from bicarbonate alkaline to alkaline earth. Magmatic CO_2 that ascends through faults dissolves into aquifers and is titrated into bicarbonate ions by interactions with the volcanic rocks (D'Alessandro et al., 1997b). This process results in the bicarbonate ion being the dominant anion in almost all aquifers, and its concentration is positively correlated with the total dissolved salt content (TDS). The strongest HCO_3 enrichment is observed in the most fractured and seismically active areas (Paternò-Belpasso to the southwest and Zafferana-S. Venerina to the east) (Anzà et al., 1989; Allard et al., 1997; D'Alessandro et al., 1999; Brusca et al., 2001), accompanied by significant enrichment in magma-derived He.

Besides the CO_2-derived bicarbonate ion, Cl^- and SO_4^{2-} can be locally abundant. Liotta et al. (2016) suggest that Cl- and S-bearing plume gases are the main controllers of the Cl^- and SO_4^{2-} contents in groundwater via meteoric scavenging.

In thinner regions of the volcanic pile, the local contribution of thermal brines coming from the sedimentary basement to the shallow aquifer results in relative enrichments in Na and Cl. This is particularly evident in the Salinelle area of Paternò, Adrano, and Bronte (Aiuppa et al., 2002) and, in the eastern sector, at Acireale, where the composition of the S. Venera thermal spring is heavily affected by Salinelle-like water ascending from the sedimentary basement and characterized by high Na, Li, B, and Cl contents. The existence of a hydrothermal system hosted within the sedimentary basement was hypothesized by Chiodini et al. (1996) from geothermometric estimations based on the chemical composition of gases emitted from the mud volcanoes of Paternò.

In the eastern basin, groundwaters flowing within the Chiancone volcaniclastic formation are enriched in Cl and SO_4 relative to the typical Etnean composition. This is probably due to leaching of S-bearing secondary minerals contained in the volcaniclastic deposits of this formation (Ferrara and Pennisi, 1993). Aiuppa et al. (2003) further considered that Cl and SO_4 enrichment could be ascribed either to a small seawater contribution, particularly for sites near the coast, or to the leaching of fertilizers containing NH_4, Ca, and SO_4.

The spatial distribution of many physicochemical parameters is not homogeneous in the Etnean aquifer; for example, groundwaters flowing in the southwestern aquifer are hotter and more saline than those in the eastern aquifer. According to Brusca et al. (2001), these differences can be

ascribed to differences in the hydrogeological characteristics (longer residence time and flow pathways, and lower rainfall) between the two basins. Indeed, a longer residence time would enhance the extent of leaching, while rainfall would lower the concentrations of chemicals. Moreover, given the close relationship between CO_2-derived bicarbonate and TDS, the spatial distributions of salinity and major and trace elements are mainly controlled by the pathways by which volcanic CO_2 ascends, which occur mostly along the tectonic structures in the southern and eastern flanks of the volcano (Brusca et al., 2001).

Methods

Periodic sample collection and analysis

Chemical data from 11 groundwater sampling sites located mainly on the eastern and southwestern flanks of Mt Etna are discussed here. These sampling sites belong to the INGV network of wells, springs, and drainage galleries that have been monitored starting from the 1990s as part of surveillance programs aimed at identifying possible relationships between variations of chemical and physicochemical parameters and volcanic activity.

The data were obtained from monthly sampling, and cover a period of about 10 years (2005–2016). Physicochemical parameters such as the water temperature, pH, and conductivity were measured. Samples for determining the contents of major elements were collected and stored in LDPE (low-density polyethylene) bottles. Ion chromatography with a suppresser and conductivity detector was applied to unfiltered samples for anions (F, Cl, NO_3, and SO_4) and to filtered (using 0.45-µm cellulose acetate filters) and acidified (using HNO_3) samples for cations (Na, K, Ca, and Mg). Alkalinity was determined by titration with 0.1 N HCl. The analytical precision was always better than 5% for each analyzed species, and the ion balance (i.e., the difference between the sum of cations and sum of anions) was always within 3%.

Continuous data were recorded at the Ponteferro and Primoti stations by continuous geochemical monitoring stations belonging to the ETNAACQUE network of INGV. These stations are able to make hourly measurements directly in the water of the temperature (NTC 10K; range=0–100°C, precision=±0.1°C), electric conductivity (customized four-electrode sensor AISI316; range=0–4000 µS, precision=±10 µS), total dissolved gas pressure (TDGP; customized pressure sensor MPX2100 AP PTFE membrane interfaced) (De Gregorio, 2005), and phreatic level (STS sensor; range=0–2.5 bar, precision=±0.25% of full scale). The data were sent once daily to the INGV acquisition center in Palermo via a GSM connection.

Results

Main chemical features

The chemical and isotope compositions, temperatures, and pH values of the sampled wells and springs are listed in Table 1. The general physicochemical and isotopic characteristics of the Mt Etna aquifer have been discussed previously (Anzà et al., 1989; Aiuppa et al., 2000; Brusca et al., 2001; Liotta et al., 2016), and therefore only a brief outline is given here. A wide chemical variability characterizes both the whole aquifer and each sampling site over time, as observed in the triangular diagram of Figure 2 that shows the relative contents of HCO_3^-, Cl^-, and SO_4^{2-}measured in samples obtained in periodic campaigns. The chemical compositions of samples collected during a large-scale survey (Parello et al., 2001) are reported for comparison. Additionally, the Cl/SO_4 ratio of local rainwater is plotted (Calabrese et al., 2011), which has been mainly ascribed to the interaction between clouds and acidic gas species in the volcanic plume (Liotta et al., 2016). Note that the samples share a composition ranging from HCO_3-rich to SO_4-rich, with a variable shift toward the Cl^- corner of the triangular diagram. The composition of samples plotting close to the HCO_3 corner is mainly due to the magmatic CO_2-driven dissolution of volcanic rocks. Moreover, there is a clearly variable contribution of Cl-rich fluids, which is typically attributable to the Salinelle area of Paternò and the S. Venera thermal springs. This part of the triangular diagram is dominated by samples from the southern sector of the volcano, collected in the area between Adrano and Belpasso, where CO_2-rich and slightly thermal waters outflow. The contribution of Cl-rich fluids coming from the underlying hydrothermal reservoir varies both spatially and temporally, as observed at spring s63bis located in the Paternò area, whose composition—which is typical of groundwater flowing in volcanic rocks—is variably affected by Cl^--rich fluids of sedimentary origin. Moving toward the SO_4^{2-} corner, the observed enrichment in SO_4 can be ascribed to the contribution of fluids related to human activities, in particular to the use of SO_4- and NO_3-rich fertilizers or farm sewage, as suggested by Brusca et al. (2001).

Figure 3 shows that contributions from fertilizers or farm sewage are evident in some samples from the s65 and Acqua Rossa sites, in that they also have higher NO_3 contents. Further enrichment in SO_4—not paralleled by NO_3 (Figure 3)—is specific for the samples collected at the Ilice, p31, and Primoti wells, site s26, and the Rocca Campana drainage galleries. SO_4 at these sites could originate from the dissolution and oxidation of hydrothermal S-bearing minerals contained in older deposits of ancient eruptive centers or, more likely, to a significant contribution of plume-affected rainwater

(Liotta et al., 2016). This variability can also be observed in the scatter plot of Na versus Cl in Figure 4. The water samples in this plot exhibit varying contributions of waters with different Na and Cl relative contents, which represents evidence that the circulation of water bodies with different compositions is controlled by either rock dissolution or the contribution of saline fluids.

The chemical composition fluctuates for some sites (i.e., Ilice, s65, s59, s26, and Primoti) during the observation time period, from HCO_3-rich to Cl- and SO_4-rich, along a virtual mixing line between the two points representing the local rainwater and rock leaching, respectively (Figure 2). Figure 5a shows the time trends of the concentrations of Cl, SO_4, and NO_3 measured at two sites on the southern flank (s65 and s59) along with their HCO_3 contents. The trends of the two parameters are approximately opposite, showing a decrease in the HCO_3 contents until early 2009, followed by an increase until late 2013, paralleled by simultaneous decreases in the contents of Cl, SO_4, and NO_3, while the trends are finally reversed in late 2013.

The composition of the s26 drainage gallery is characterized by marked temporal variability during the observation period, with the water composition changing from HCO_3-richer to Cl- and SO_4-richer (Figure 2). This is clearly evident in the scatter plot in Figure 5b of the HCO_3 contents measured at sites s26 and Primoti which drain two different levels of the same water body—versus the sum of the Cl, SO_4, and NO_3 contents. In this case a progressive decrease in HCO_3 contents is observed until early 2009, while the Cl, SO_4, and NO_3 contents are approximately constant. After 2009 the two parameters show similar behaviors over the same periods, although they do not co-vary closely: a phase of increase during 2009 and 2010 is followed by a gradual decrease until early 2013, after which the two parameters increase again until late 2014, although at different rates.

Discussion

Significant variations in saline content and composition are observed in the Etnean aquifer during the 10-year observation period (2005–2015) analyzed in this study. To shed light on the possible causes of these changes, we first consider the role of variable rainfall, followed by the effects of the dynamics of the volcano.

Influence of rainfall on the volcanic aquifer

Changes in rainfall usually affect the dynamics of hydrological systems, mainly influencing the yields of both springs and drainage galleries and the water-table height of unconfined aquifers. The height of the water table frequently appears to be directly correlated with meteoric recharge, with

other factors such as temperature, hydraulic conductivity, vegetation, and hydraulic gradients being less important (Aphale and Tonjes, 2010). In particular, the water-table head is strongly correlated with the cumulative difference in the monthly rainfall relative to a previous period (6, 12, or 24 months, depending on the lengths of the hydrological pathways) (Aphale and Tonjes, 2010; Van Gaalen et al., 2013). On the other hand, the change in the rainfall can also affect the chemical composition and salinity of hydrological systems (D'Alessandro et al., 2011).

To ascertain the effect of rainfall on the volcano aquifer, we consider the data on rainfall provided by the meteorological network operating in Sicily (Regione Siciliana; www.osservatorioacque.it). These data are compared with the water chemistry analyzed at some of the sites. The time trends of the concentrations of Cl, SO_4, and NO_3 measured at sites s65 and s59 are plotted in Figure 6 as normalized values. This graph also shows the rainfall measured in Pedara village (Regione Siciliana; www.osservatorioacque.it) as the cumulative departure of monthly difference relative to the mean over the previous 18 months. The figure shows significant variations in rainfall during the studied period. These variations appear to be roughly correlated with those observed for the Cl, SO_4, and NO_3 contents, thus indicating that these anions are mainly controlled by the circulation of shallow water. Although both parameters show a gross covariation over the studied period, a closer look reveals some discrepancies (dashed rectangles in Figure 6) that suggest the water chemistry at spring s65 and well s59 is affected by additional factors other than the rainfall. To quantify and correct for the effect of the rainfall on the variations of Cl, SO_4, and NO_3 contents at s59, we applied the following procedure:

1. Computing the normalized values of both the rainfall and the chemical concentrations as $\left(Z = \frac{x - mean}{\sigma}\right)$, where Z is the normalized value, x is the raw value, and σ is the standard deviation.
2. Subtracting the normalized values of the rainfall from the normalized concentrations of Cl, SO_4, and NO_3.

The obtained series is plotted in Figure 6 which clearly shows that the residual Cl, SO_4, and NO_3 contents are unrelated to the variations in the rainfall. A value of zero means that there is no effect additional to the rainfall, while negative values mean that the contribution of water rich in Cl, SO_4, and NO_3 is lower than what would be expected from the influence of the rainfall, and vice versa for positive values.

Figure 7 compares the normalized rainfall values with the water level measured daily within the catchment of site s65. A close relationship is evident, related to the direct effect of meteoric precipitation on the water level, if we exclude specific periods when the trend of the water level

differs from that of the rainfall (dashed rectangles in Figure 7). Similarly to what is observed for the water chemistry in Figure 6, an additional cause other than the rainfall needs be invoked to explain the time variations of the water level during specific periods.

Figure 8 compares the normalized values of the rainfall (expressed as the cumulative difference relative to the mean rainfall over the previous 18 months; Figure 8a) and the yield and TDGP measured at the s26 drainage gallery and Primoti well, respectively; Figure 8b). As already observed by Mattia et al. (2015), the variations of the rainfall observed during the studied period clearly affect with a delay of a few months both the yield measured at the drainage gallery s26 and the TDGP measured at Primoti well, although a closer look does reveal some discrepancies. As highlighted also for the s65 catchment, an additional source needs to be identified. To determine the influence of the rainfall on the yield and TDGP, we applied the same procedure described for the Cl, SO_4, and NO_3 contents at site s65. The cumulative series of normalized values of the rainfall were subtracted from the cumulative series of both the yield and TDGP normalized values by considering a 4-month shift between the signals. The corrected series is plotted in Figure 8c, which represents the residual yield and TDGP unrelated to variations in the rainfall.

Time trends

As observed in the triangular diagram of Figure 2, most sites show a temporal variability during the monitored period that would suggest contributions of water types with different chemical signatures to the spring output, and that their mixing proportion varies over time. The CO_2-rich groundwater, which interacts extensively with the volcanic rock, mixes with water circulating at shallow levels (i.e., meteoric water variably polluted during soil leaching). Moreover, most sites also display changes in the concentrations of chemicals. In particular, the increase in the NO_3 content is paralleled by a general decrease in the salinity (generally co-varying with the HCO_3 content), which probably characterizes water circulation at shallow levels that is affected by pollution from agriculture. The extent of mixing between these different types of water changes over time, probably as an effect of changes in circulation patterns, involving the transfer of water from/to water bodies with different compositions. This variation in water circulation can probably be ascribed to either the periodicity of the rainfall or to events of slow ground deformation that modify the fluid pressure distribution within the saturated levels of the volcanic edifice (Mattia et al., 2015). In order to quantify the proportions of the shallow and deep waters at each monitored site, we assume that all of the HCO_3 content measured in collected samples derives from the dissolution and hydrolysis of CO_2, whereas the contents of SO_4, Cl and NO_3 come from fertilizers, saline fluids, or

plume-affected rainwater (Liotta et al., 2016). This is an oversimplification, but allows changes in water circulation to be highlighted, eventually coupled to changes in the input of CO_2 and consequent rock leaching. In general, the total saline content (quantified as the TDS) co-varies with the HCO_3 content, since the latter is the dominant anion in the Etnean groundwater. The fraction of the water rich in Cl, SO_4, and NO_3 can be computed for each sampling campaign and at every site by assuming a simple binary mixing between two end members characterized by the highest and lowest $HCO_3/(Cl+SO_4+NO_3)$ ratios, respectively, identified as the volcanic and $Cl/SO_4/NO_3$-polluted (CSN) end members within the whole time series at each specific site:

$$(R)_{mix} = \varphi R_{\min} + (1-\varphi) R_{\max} \qquad [1]$$

where R_{mix}, R_{min}, and R_{max} are the $HCO_3/(Cl+SO_4+NO_3)$ ratio in the measured mixture and the minimum and maximum values of this ratio measured in the whole time series (from 2005 to 2015), respectively, and φ is the fraction of the Cl, SO_4, and NO_3 contents in the mixture contributed by the CSN end member, which can be expressed as

$$\varphi = \frac{([\mathrm{Cl}]+[\mathrm{SO_4}]+[\mathrm{NO_3}])_{\mathrm{CSN}} \cdot f}{([\mathrm{Cl}]+[\mathrm{SO_4}]+[\mathrm{NO_3}])_{mix}} \qquad [2]$$

where f is the fraction of the CSN end member, and $([Cl]+[SO_4]+[NO_3])_{mix}$ and $([Cl]+[SO_4]+[NO_3])_{CSN}$ are the concentrations of Cl, SO_4, and NO_3 in the mixture and the CSN end member, respectively, identified in the considered time series according to the linear relationship between the $HCO_3/(Cl+SO_4+NO_3)$ ratio and $1/(Cl+SO_4+NO_3)$ expected for binary mixing (Albarède, 1995) and exemplified in Figure 9 for site s65.

Once the f fraction is obtained, the HCO_3 amount provided by the CSN end member is easily obtained as $f \cdot [HCO_3]_{CSN}$, where $[HCO_3]_{CSN}$ is the HCO_3 concentration in the CSN end member obtained from

$$[\mathrm{HCO_3}]_{\mathrm{CSN}} = R_{\min} \cdot ([\mathrm{Cl}]+[\mathrm{SO_4}]+[\mathrm{NO_3}])_{\mathrm{CSN}} \qquad [3]$$

This makes it possible to compute the fraction of HCO_3 strictly related to the dissolution and hydrolysis of gaseous CO_2, and to track how the input of CO_2 into the aquifer varies over time. The concentration of HCO_3 contributed by the CSN end member can only be estimated since the end members are not unequivocally defined. Nevertheless, there are still significant time trends that make it possible to quantify the amount of carbon dissolving into the aquifer over time.

Figure 10 shows the time trends of HCO_3 contents exceeding the fraction related to the mixing with the CSN end member, as computed using Equation 3, at selected sites on the southern flank: s65, s59, s63bis, and Romito. This figure reveals similar trends at the different sites, with variations in the HCO_3 content related to the CO_2 dissolution (HCO_3 excess) ranging from about 4 to 14 meq/l, on average. The computed CO_2 excess is highest at s63bis, Solicchiata (not shown), and

Romito, whereas sites s59 and s65 are the least affected by the input of volcanic CO_2; the contribution of the CSN end member is more evident at these latter sites (see Figure 5).

In contrast to what was observed on the southern flank, the temporal patterns of CO_2 excess in water sites sampled on the eastern flank do not show a uniform behavior. As evident in Figure 11, each site on the eastern flank shows a specific temporal pattern, with only partial matching for limited periods with other sites. This can be attributed to the existence of multiple faults on the eastern flank that outline different blocks with different kinematics (Azzaro et al., 2013). This would affect also the gas emission along these different structures during the history of the volcano. Among the sites sampled on the eastern flank, s26 shows the highest values of the HCO_3 excess, followed by S. Giacomo, while p31, Rocca Campana, and Ilice have the lowest HCO_3 excess or, in other words, the lowest input of gaseous CO_2 due to volcanic degassing processes.

The time trends of the HCO_3 excess at s26 and Primoti, computed using Equations 1–3, are illustrated in Figure 12, along with the residual yield and TDGP at the same sites. The HCO_3 excess computed at the s26 and Primoti sites show similar values and temporal patterns, which is probably due to their closeness and the sharing of a common hydrological basin. Moreover, the HCO_3 excess also shows a definite relationship with the CO_2 soil emissions in the same area, as expected from the process of hydrolysis of gaseous CO_2 in groundwater (Mattia et al., 2015). Some similarities are also evident when the HCO_3 excess is compared with the residual yield and TDGP, with consistent behaviors that represent evidence of a common source mechanism for the CO_2 degassing and variations in water circulation. It must be underscored that the HCO_3 excess, residual yield, and TDGP are independent parameters, because the HCO_3 excess is corrected for any influence of water flow related to variable rainfall input or other causes, while the residual yield and TDGP are corrected for rainfall effects.

While the different sites on the eastern flank show different temporal patterns, we considered it useful to compare the sum of all the time series with the total HCO_3 excess computed for the sites from the southwestern flank. The resulting series are shown in Figure 13. Although single sites show specific behaviors, mostly on the eastern flank, homogeneous trends arise from the observation of the whole record, with synchronous variations in both sectors of the volcano. The main phases when the HCO_3 excess has been increased relative to the running average value have been recorded in 2005, 2007, 2009, and 2011, and during 2013–2015, which is particularly evident on the southern flank.

Changes in fluid circulation: the role of volcano dynamics

As shown in Figures 6 and 8, the temporal changes in both the water chemistry and the yield/water level/TDGP at selected sites are to some extent independent of the effect of the rainfall. The residual values of chemical or flow parameters present negative or positive values, according to their excess or deficiency with respect to that expected from rainfall. This would mean that part of the chemicals could be contributed or subtracted by water flowing from or toward adjacent water bodies. In particular, for site s59, the sum of the concentrations of Cl, NO_3, and SO_4 corrected for the effect of the rainfall (i.e., the residual contents of Cl, SO_4, and NO_3) shows slightly positive values during 2005 and 2006 and in 2008, marked negative values in 2009 and 2011, and again positive values during 2014 and 2015. Significant changes in the residual yield of the s26 drainage gallery and in the TDGP at the Primoti well are also observed over the investigated period (Figure 8). In detail, progressive decreases in the residual yield and TDGP values are evident from 2005 to 2008, followed by increases in 2009 and steady values until 2012. The decreases observed from 2013 are then sharply reversed in 2015.

The increase or decrease in the flow rate (or TDGP), independently of the rainfall, implies that the flow pathway of water has been diverted so that the water is now progressively coming from or flowing toward adjacent water bodies, which produces a specific water composition. This would explain the parallel changes in water chemistry observed during the same periods (Figure 5). This mechanism could be extended over the whole volcano, where marked heterogeneities (both vertical and horizontal) characterize the water chemistry. These changes in the flow pathways can be reliably ascribed to differential changes in the pore pressure gradients in the volcanic edifice, according to Darcy's law (e.g., Whitaker, 1986).

There are two principal types of mechanism underlying changes in fluid pressure in a volcanic edifice:

1. Stress-related mechanisms, such as compaction and tectonic loading.
2. Volume changes, involving the input of magmatic fluids or hydrothermal expansion, water or gas withdrawal, or changes in meteoric input (Newhall et al., 2001; Thomas et al., 2004).

These two mechanisms are taken into account in the relationship proposed by Roeloffs and Linde (2007), which links the variations of fluid pressure to both the change in volumetric crustal strain (in the absence of fluid flow) and the change in the mass of fluid.

The relationship between variations of crustal strain and related fluid pressure and the changes in the yield of the s26 drainage gallery and the nearby Primoti well has been recently demonstrated by Mattia et al. (2015) for the period 2008–2013. However, they disregarded the eventual effect of the change in the mass of fluid on the computed fluid pressure.

Considering the described relationship between crustal strain and fluid pressure and its subsequent release as fluid flow, we assume that the variations in fluid circulation—indicated by changes in the chemical composition—can be reliably correlated with simultaneous changes in the geodetic strain of the volcano. We also intended to verify the relationship between these changes in fluid circulation and the increased CO_2 input into the aquifer, as indicated by the HCO_3 excess.

There is a wealth of data available on ground movements of Mt Etna, which record the various phases of inflation and deflation of the volcano, as well as the progressive acceleration of its eastern flank toward the sea (Bonforte et al., 2008; Bonaccorso et al., 2011; Bruno et al., 2012 and references therein). The ground movements are undoubtedly related to the phases of pressurization and depressurization preceding and following the different eruptions, but also to the complex geometry of the eastern flank, which is dissected into blocks characterized by different kinematics (Azzaro et al., 2011).

A complex scenario developed after the eruption during 2002 and 2003, with the eastward movement of the eastern flank representing the first-order deformation, and phases of uplift or subsidence being observed on the scale of the entire edifice (Bonaccorso et al., 2006; Neri et al., 2009; Bruno et al., 2012). An overall east–west extension prevailed at shallow depth, mostly controlled by the eastward movement of the eastern flank. This exceptional extension probably caused the opening of eruptive fractures into which the magma intruded passively and fed the eruptions during 2004 and 2005 and in 2006 (Alparone et al., 2013). This scenario, which mainly affects the eastern flank of the volcano, can explain the progressive decrease in the residual fluid pressure (i.e., decrease in the residual yield) observed at the s26 drainage gallery until 2008 (Figure 12). Otherwise, no significant parameter variations (i.e., contents of Cl, SO_4, and NO_3) related to the residual water flow are evident on the southern flank until 2009 (Figure 6). Actually, detrended data of the residual yield and TDGP on the eastern flank reveal a phase of increased values from late 2005 to early 2006 (Figure 12). Values of the HCO_3 excess higher than the running average were measured in 2005 on both the southern and eastern flanks of the volcano (Figure 13). This can be attributed to a phase of recharge of the volcano reservoir that was detected in GPS surveys (Bonforte et al., 2008) and from seismicity and gravity data (Carbone et al., 2008), and which heralded the onset of the eruption several months later in July 2006.

Another phase of increased HCO_3 excess, related to increased CO_2 input, occurred in 2007 (Figure 13), when several episodes of explosive activity and lava fountaining occurred at the summit area of the volcano (Andronico et al., 2008). Several cycles of inflation-deflation in 2007 and until the onset of the May 2008 eruption were paralleled by analogous variations of the CO_2/SO_2 ratios in the plume and volcanic tremor, each characterized by a lava fountaining episode

(Aiuppa et al., 2010). The progressive pressurization of the central conduit system (1.0–2.8 km a.s.l.) by CO_2-rich magma ascending from depth may explain the increase in the carbon content of groundwater. However, the residual yield and TDGP on the eastern flank reveal consistent increases in the detrended values (Figure 12), whereas an almost monotonic decreasing trend is probably associated with to the flank spreading. Conversely, on the southern flank, no significant change in water chemistry can be ascribed to changes in water circulation (Figure 6). This different behavior would suggest that changes in water circulation during that period are effects of phenomena that only affect the eastern flank of the volcano.

According to geodetic and seismic data, the period from late 2006 to May 2008 (i.e., the inflation phase preceding the eruption that started on May 13, 2008) is characterized by a change in the areal distribution of the shear strain rate relative to the two preceding periods of inflation during 2003 and 2004 and during 2005 and 2006 (Bruno et al., 2012). Indeed, during the first two inflation periods, the shear strain rate (which is mainly attributed to the southeastward subsidence of the eastern flank; that is, nonvolcanic processes) was focused on the upper eastern flank, bounded by the northeast rift and the Timpe fault system. In contrast, during the latter inflation period (before the 2008 eruption), the shear strain rate was focused along the Pernicana Fault, while the area involved in sliding on the eastern flank enlarged to include the upper flank (Bruno et al., 2012). Moreover, whereas the previous phases during 2003 and 2004 and during 2005 and 2006 were marked by changes in the shear strain rate (interpreted as being related to the source of inflation) and also involved the western flank, from 2006 to 2008 they only affected the eastern flank. The described changes in the strain distribution that occurred since December 2006 would have also affected fluid movement and groundwater circulation only on the eastern flank.

During the first months of 2009, a new change in water circulation was recorded in the monitored wells and springs. Figures 6 and 12 demonstrate marked changes in water chemistry, residual yield, and TDGP, while an increase in the HCO_3 excess is evident in both sectors of the volcano in Figure 13. The spring of 2009 marked a significant change in many geophysical and geochemical parameters, as discussed recently by Mattia et al. (2015). Indeed, from April 2009, the GPS data, strain release, and number of volcanotectonic earthquakes as well as the amplitude of long-period events changed their trends almost concurrently, which was not related temporally to any eruptive activity. These data, along with the simultaneous increase in CO_2 emissions from the soil, have been attributed to gas overpressure in the shallow feeding system.

2011 heralded another phase of change in water circulation in both sectors of the volcano, as indicated by the water chemistry (Figure 6) and higher values of the residual yield and TDGP (Figure 12). At the same time, a marked increase in the HCO_3 excess is evident in groundwater

(Figure 13). This period was characterized by several episodes of lava fountaining (25 episodes from January 2011 and April 2012 (Behncke et al., 2014), which led to the building of the new southeast crater. Several deep seismic swarms were observed throughout this phase in the southwestern flank, which marked the replenishment of the deep-to-intermediate levels of the plumbing system (Patanè et al., 2013). It is worth noting that the values of the HCO_3 excess became increasing larger on the southern flank than on the eastern flank during this period, in contrast to them almost overlapping before 2010.

Further changes in water circulation—after correction for the effect of the rainfall—have been observed during 2014 and 2015 in both the s26/Primoti system and in the Paternò area (Figures 6 and 12). However, the HCO_3 excess has remained high since 2013. Actually, several episodes of lava fountaining occurred at the new southeast crater from January 2011 to April 2013, which has resulted in the emission of up to 95 Mm^3 of lava (Bonaccorso and Calvari, 2013). 2014 was mostly characterized by Strombolian activity, and by an episode of lava fountaining in November 2014 (Bonforte and Guglielmino, 2015).

According to the arguments presented above, the chemical composition of groundwater and its gas content can change over time as an effect of volcano dynamics, in a broad sense. In particular, it appears evident that, regardless of the occurrence of eruptions, the water circulation pathways can be altered by pressure changes in the volcanic edifice caused by the volcanic fluid overpressure within the feeding system and/or the geodetic strain affecting the volcano. The chemical variations are specific to single sampling sites, and they depend on the vertical and spatial heterogeneity of the volcanic aquifer, made of superimposed water bodies, and characterized by different temperature, salinity, and chemical composition. In any case, the changes in chemical composition are to a large extent determined by mixing between a meteoric end member, characterized by lower HCO_3 content and the prevailing Cl, SO_4, and (sometimes) NO_3 ions, deriving from plume contribution to the rainfall or from anthropogenic pollution, and a volcanic end member, which is typically rich in HCO_3. The contribution of the meteoric end member is largely controlled by the rainfall periodicity, but once the effect of the rainfall has been apportioned, a residual effect can be observed. Similarly, at the few sites where it can be measured, even the water level, yield, and TDGP show a residual signal that is independent of the rainfall. The ultimate cause of these residual effects is likely to be the variation in the distribution of fluid pressure gradients over the volcanic edifice. These gradients can change according to the spatial distribution of the geodetic and seismic strain, as well as with the mass transfer of fluids. The correspondence between the frequent increases in the HCO_3 excess—which represents the amount of carbon entering the volcanic aquifer from depth—and the changes in water circulation suggested by the marker parameters (Figures 6 and 12) represents

evidence of a primary role of volcanic fluids. Indeed, volcanic fluids emitted during the described phases of increased volcanic activity have evidently permeated the volcanic edifice along preferential pathways, partially dissolving into the aquifer, and could have enhanced local pressure buildups. Such pressure increases could frequently induce both ground deformation and changes in the flow pathways of groundwater, leading to the observed changes in water composition.

Conclusions

Our analysis of the 10-year record of the major-ion composition in the Etnean aquifer has shed light on some of the processes affecting both water chemistry and circulation. The water chemistry is greatly affected by variable mixing between water end members characterized by different composition and salinity. The volcanic end member is rich in HCO_3 and low in Cl, SO_4, and NO_3; the latter instead characterize the meteoric-polluted end member. The relative mixing proportions of these two water types change at single sites mainly due to the variability of the meteoric input. The yield or the TDGP measured at selected sites also change accordingly. Nevertheless, once the signals are corrected for the effect of the rainfall, the residual effect can be attributed to differences in the variations of fluid pressure within the volcanic edifice, due to volcano dynamics. Regardless of the mechanism underlying the variations in the water circulation, we have retrieved the fraction of dissolved carbon unrelated to the mixing between the volcanic and meteoric (i.e., CSN) end members, thus obtaining the residual HCO_3 that is directly related to variations in the input of volcanic CO_2 into the aquifer.

The phases of increased input of CO_2 into the aquifer are synchronous in the two areas most affected by volcanic degassing: the Paternò and the Zafferana-S. Venerina areas; moreover, they frequently occur simultaneously with the chemical changes related to water circulation, such as in 2009 and during 2011–2013. The simultaneous occurrence of a change in water circulation in wells and springs located in different sectors of the volcanic edifice is consistent with a phenomenon occurring on the scale of the volcanic edifice. This would represent evidence that the variations of fluid pressure which induce the variations in the water flow pathways are caused by volcanic gas overpressure. Moreover, gas overpressure due to magma boiling along the multilevel plumbing system has been interpreted as a major cause of differential ground deformation of the volcano (Aloisi et al., 2011).

Captions

Figure 1 - Mt Etna sketch map showing the locations of the sampling sites. The morphostructural base map is modified from Branca et al. (2011, 2013).

Figure 2 - Triangular diagram of HCO_3, Cl, and SO_4 for the monitored sites. Concentrations are in milligrams per liter. The field representative of the Cl/SO_4 ratios in rainwater (Calabrese et al., 2011) and the data from Parello et al. (2001) are plotted for comparison.

Figure 3 - Scatter plot of SO_4 versus NO_3. The field representing water circulating within the Chiancone formation is indicated in gray. The straight line indicates the NO_3/SO_4 ratio that is probably attributable to human activities (e.g., fertilizers or farm sewage). Symbols as in Figure 2.

Figure 4 - Scatter plot of Cl versus Na. Symbols as in Figure 2. The straight line represents the Na/Cl ratio in the Salinelle fluids.

Figure 5 - Time trends of Cl, SO_4, and NO_3 contents versus HCO_3 contents at sites s65 and s59 (a) and at sites s26 and Primoti (b). Symbols as in Figure 2.

Figure 6 - a) Time trends of the sum concentrations of Cl, SO_4, and NO_3 at sites s56 and s59, and the rainfall (expressed as the cumulative difference relative to the mean over the previous 18 months). b) Residual contents of Cl, SO_4, and NO_3 at s59, as obtained by subtracting the normalized rainfall values from the normalized contents of Cl, SO_4, and NO_3 at s59.

Figure 7 - Time trends of the normalized rainfall (expressed as the cumulative difference relative to the mean over the previous 18 months) and daily data for the water level at site s65.

Figure 8 - a) Time trends of the normalized rainfall (expressed as the cumulative difference relative to the mean over the previous 18 months); dashed line indicates a forward shift of 4 months. b) Time trends of the yield measured at s26 and TDGP at the Primoti well. c) Residual yield and TDGP values, as obtained by subtracting the normalized rainfall values from the normalized yield and TDGP values.

Figure 9 - Scatter plot of $HCO_3/(Cl+SO_4+NO_3)$ versus $1/(Cl+SO_4+NO_3)$. The straight line represents binary mixing.

Figure 10 - Time trends of the HCO_3 excess computed using Equations 1–3 at sites s59, s65, S63bis, and Romito, which are in the southwestern basin.

Figure 11 - Time trends of the HCO_3 excess computed using Equations 1–3 at sites s26, S. Giacomo, Ilice, p31, and Rocca Campana, which are in the eastern basin.

Figure 12 - a) Time trends of the HCO_3 content at site s26 and the HCO_3 excess at sites s26 and Primoti. b) Residual yield and TDGP values (black lines) and detrended values (red lines).

Figure 13 - Time trends of the average HCO_3 excess (normalized values) in the southwestern sector (red line) and in the eastern sector (blue line).

Acknowledgements - The data set discussed in this paper was obtained from surveillance programs of Mt Etna performed by INGV and funded by the Italian Civil Protection Department. This study has also benefited from the Agreements INGV-DPC 2012-15.

We also wish to thanks the firm “acque Ponte di Ferro” of Ing. Sarino Pavone for providing data of water yield measured at the Ponteferro drainage gallery.

References

Aiuppa, A., Federico, C., Giudice, G., Giuffrida, G., Guida, R., Gurrieri, S., Liuzzo, M., Moretti, R., Papale, P. (2009) The 2007 eruption of Stromboli volcano: Insights from real-time measurement of the volcanic gas plume CO2/SO2 ratio Journal of Volcanology and Geothermal Research, 182, 221–230, doi:10.1016/j.jvolgeores.2008.09.013

Aiuppa, A., Burton, M., Caltabiano, T., Giudice, G., Gurrieri, S., Liuzzo, M., Muré, F., Salerno, G. (2010) Unusually large magmatic CO_2 gas emissions prior to a basaltic paroxysm, Geophysical Research Letters 37 (17), L17303

Aiuppa, A., Allard, P., D'Alessandro, W., Michel, A., Parello, F., Treuil, M. and Valenza, M., Mobility and fluxes of major, minor and trace metals during basalt weathering and groundwater transport at Mt. Etna volcano (Sicily). Geochim. Cosmochim. Acta, 64 (11), 2000, 1827-1841.

Aiuppa, A., Brusca, L., D’Alessandro, W., Giammanco, S.,Parello, F., 2002. A case study of gas-water-rock interaction in a volcanic aquifer: the south-western flank of Mt. Etna(Sicily). In: Stober, I., Butcher, K. (Eds.), Water-Rock Interaction in Hydrogeology. Kluwert Academic, Nederlands,pp. 125–145.

Aiuppa, A., Bellomo, S., Brusca, L., D’Alessandro, W., & Federico, C. (2003). Natural and anthropogenic factors affecting groundwater quality of an active volcano (Mt. Etna, Italy). *Applied Geochemistry, 18*, 863–882.

Albarède, F., Introduction to Geochemical Modeling., Cambridge Univ. Press, New York, 1996.

Allard, P., J. Carbonnelle, D. Dajlevic, J. Le Bronec, P. Morel, M. C. Robe, J. M. Maurenas, R. Faivre-Pierret, D. Martin, J.C. Sabroux, and P. Zettwoog, Eruptive and diffuse emissions of CO_2 from Mount Etna, *Nature,* 351, 387-391, 1991.

Allard, P., Endogenous magma degassing and storage at Mount Etna, *Geophys. Res. Lett*., 24(17), 2219-2222, 1997.

Allard, P., Jean-Baptist,e P., D'Alessandro, W., Parello, F., Parisi, B. and Flehoc, C., Mantle-derived helium and carbon in groundwaters and gases of Mount Etna, Italy. Earth Planet. Sci. Letters 148, 1997, 501-516.

Aloisi, M., Mattia, M., Monaco, C., and Pulvirenti, F., 2011. Magma, faults, and gravitational loading at Mount Etna: The 2002-2003 eruptive period. Journal of Geophysical Research-Solid Earth 116.

Alparone, S., Bonaccorso, A., Bonforte, A., and Currenti, G., 2013. Long-term stress-strain analysis of volcano flank instability: The eastern sector of Etna from 1980 to 2012. Journal of Geophysical Research-Solid Earth 118, 5098-5108.

Andronico D.,Cristaldi A., Scollo S. (2008) The 4-5 September 2007 lava fountain at South-East Crater of Mt Etna, Italy Journal of Volcanology and Geothermal Research 173 (2008) 325-328 doi:10.1016/j.jvolgeores.2008.02.004

Anzà, S., G. Dongarrà, S. Giammanco, V. Gottini, S. Hauser, and M. Valenza, Geochimica dei fluidi dell’Etna: Le acque sotterranee,
Mineral. Petrogr. Acta, 32**,** 231-251, 1989.

Aphale, O. and D.J. Tonjes. 2010. Recharge and head: preliminary findings using a long-term data set. Long Island Geologists' Abstracts Collection. Stony Brook University: Department of Geosciences; Stony Brook, NY. http://hdl.handle.net/1951/49439.

Azzaro, R., A. Bonforte, S. Branca, and F. Guglielmino (2013), Geometry and kinematics of the fault systems controlling the unstable flank of
Etna volcano (Sicily), J. Volcanol. Geotherm. Res., 251, 5−15.

Barberi, F., Civetta, L., Gasparini, P., Innocenti, F., Scandone, R., Villari, L., 1974. Evolution of a section of the Africa-Europe plate boundary: paleomagnetic and volcanological evidence from Sicily. Earth Planet. Sci. Lett. 22, 123–132.

Battaglia, M., C. Troise, F. Obrizzo, F. Pingue, and G. De Natale (2006), Evidence for fluid migration as the source of deformation at Campi Flegrei caldera (Italy), Geophys. Res. Lett., 33, L01307, doi:10.1029/2005GL024904.

Behncke B., Branca S., Corsaro R.A., De Beni E., MiragliaL., Proietti C. (2014) The 2011–2012 summit activity of Mount Etna: Birth, growth and
products of the new SE crater Journal of Volcanology and Geothermal Research 270 (2014) 10–21 .doi.org/10.1016/j.jvolgeores.2013.11.012

Bonaccorso, A., A. Bonforte, F. Guglielmino, M. Palano, and G. Puglisi (2006), Composite ground deformation pattern forerunning the 2004–2005 Mount Etna eruption, J. Geophys. Res., 111, B12207. doi:10.1029/2005JB004206.

Bonaccorso A. and Calvari S. (2013) Major effusive eruptions and recent lava fountains: Balance between expected and erupted magma volumes at Etna volcano. Geophysical Research Letters, vol. 40, 6069–6073, doi:10.1002/2013gl058291, 2013

Bonaccorso A., Caltabiano T., Currenti G., Del Negro C., Gambino S., Ganci G., Giammanco S., Greco F., Pistorio A., Salerno G., Spampinato S., and Boschi E. (2011) Dynamics of a lava fountain revealed by geophysical, geochemicaland thermal satellite measurements: The case of the 10 April 2011Mt Etna eruption Geophysical Research Letters, vol.38, l24307,doi:10.1029/2011gl049637, 2011

Bonforte A., Bonaccorso A., Guglielmino F., Palano M., and Puglisi G. (2008) Feeding system and magma storage beneath Mt. Etna as revealed by recent inflation/deflation cycles Journal of geophysical research, vol. 113, b05406, doi:10.1029/2007jb005334, 2008

Bonforte A. and Guglielmino F.(2015)Very shallow dyke intrusion and potential slope failure imaged by ground deformation: The 28December 2014 eruption on Mount Etna Geophys. Res. Lett., 42, 2727–2733, doi:10.1002/2015GL063462.

Bousquet, J.-C., G. Lanzafame, and C. Paquin, Tectonic stresses and volcanism: in-situ stress measurements and neotectonic investigations in the Etna area (Italy), *Tectonophys., 149,* 219-231, 1988.

Branca, S. and Ferrara, V., 2013. The morphostructural setting of Mount Etna sedimentary basement (Italy): Implications for the geometry and volume of the volcano and its flank instability. Tectonophysics 586, 46-64.

Bruno, V., M. Mattia, M. Aloisi, M. Palano, F. Cannav_o, and W. E. Holt (2012), Ground deformations and volcanic processes as imaged by
CGPS data at Mt. Etna (Italy) between 2003 and 2008, J. Geophys. Res., 117, B07208, doi:10.1029/2011JB009114.

Brusca, L., Aiuppa, A., D'Alessandro, W., Parello, F., Allard, P., Michel, A., 2001. Geochemical mapping of magmatic gaswater- rock interactions in the aquifer of Mount Etna volcano. J. Volcanol. Geotherm. Res. 108, 201–220.

Calabrese, S., Aiuppa, A., Allard, P., Bagnato, E., Bellomo, S., Brusca, L., D'Alessandro, W,. Parello F., 2011. Atmospheric sources and sinks of volcanogenic elements in a basaltic volcano (Etna, Italy). Geochim. Cosmochim. Acta 75, 7401–7425.

Capasso G., Federico C., Madonia P., Paonota A. (2014) Response of the shallow aquifer of the volcano-hydrothermal system during the recent crises at Vulcano Island (Aeolian Archipelago, Italy) Journal of Volcanology and Geothermal Research 273 (2014) 70–80. doi.org/10.1016/j.jvolgeores.2014.01.005

Caracausi A, Italiano F, Nuccio P M, Paonita A, Rizzo A (2003) Evidence of deep magma degassing and ascent by geochemistry of peripheral gas emissions at Mt. Etna (Italy): assessment of the magmatic reservoir pressure. J Geophys Res 108 (B10): 2463 doi: 10.1029/2002JB002095.

Carbone, D., Zuccarello, L., and Saccorotti, G., 2008. Geophysical indications of magma uprising at Mt Etna during the December 2005 to January 2006 non-eruptive period. Geophysical Research Letters 35.

Carbone, S., M. Grasso, and F. Lentini, Lineamenti geologici del Plateau Ibleo (Sicilia SE). Presentazione carte geologiche della Sicilia sud-orientale, Mem. Soc. Geol. It., 38, 127-135, 1987.

Chester, D.K., Duncan, A.M., Guest, J.E., Kilbum, C.R.J., 1985. Mount Etna: The Anatomy of a Volcano. Chapman & Hall, London.

Chiodini, G., D'Alessandro, W., & Parello, F. (1996). Geochemistry of the gases and of the waters discharged by the mud volcanoes of Paternò, Mt. Etna (Italy). Bulletin of Volcanology, 58, 51–58.

Chiodini, G., T. Brombach, S. Caliro, C. Cardellini, L. Marini, and V. Dietrich (2002), Geochemical indicators of possible ongoing volcanic unrest at Nisyros Island (Greece), Geophys. Res. Lett., 29(16), 1759, doi:10.1029/2001GL014355.

Chiodini G., Caliro S., Cardellini C., Granieri D., Avino R., Baldini A., Donnini M., Minopoli C.. Long-term variations of the Campi Flegrei, Italy, volcanic system as revealed by the monitoring of hydrothermal activity. Journal of Geophysical Research, vol. 115, B03205, doi:10.1029/2008JB006258, 2010

Christiansen, L. B., S. Hurwitz, M. O. Saar, S. E. Ingebritsen, and P. A. Hsieh (2005), Seasonal seismicity at western United States volcanic centers,
Earth Planet. Sci. Lett., 240, 307–321.

Claesson, L., A. Skelton, C. Grahmn, C. Dietl, M. Morth, P. Torssander, and I. Kockum (2004), Hydrogeochemical changes before and after a
major earthquake, Geololgy, 32(8), 641–644.

Day, S.J., 1996. Hydrothermal pore fluid pressure and the stability of porous, permeable volcanoes. In: McGuire, W.C., Jones, A.P., Neuberg, J. (Eds.), Volcano Instability on the Earth and Other Planets. Geol. Soc. London, Spec. Publ. No. 110, 77–93.

D'Alessandro, W., Bellomo, S., Bonfanti, P., Brusca, L., and Longo, M., 2011. Salinity variations in the water resources fed by the Etnean volcanic aquifers (Sicily, Italy): natural vs. anthropogenic causes. Environmental Monitoring and Assessment 173, 431-446.

D'Alessandro, W., S. De Gregorio, G. Dongarrà, S. Gurrieri, F. Parello, and B. Parisi, Chemical and isotopic characterization of the gases of Mount Etna (Italy), *J. Volcanol. Geotherm. Res*., 78, 65-76, 1997.

D'Alessandro, W., Federico, C., Aiuppa, A., Longo, M., Parello, F., Allard, P. and Jean-Baptiste, P., 2001. Groundwater circulation at Mt. Etna: evidences from ^{18}O, ^{2}H and ^{3}H contents. In: Proceedings of the 10th International Symposium on Water-Rock Interaction WRI-10, Balkema, pp. 485–488.

D'Alessandro, W., Inguaggiato, S., Federico, C., Parello, F., 1999. Chemical composition of dissolved gases in groundwaters from Mount Etna, Eastern Sicily. In: Armannsson, H. (Ed.), Geochemistry of the Earth's Surface. Balkema, Rotterdam, pp. 491–494.

Dall'Aglio, M., F. Pagani, and F. Quattrocchi, Geochemistry of the groundwaters in the Etna region before and after the paroxysmal phase of the eruption of December 1991: implications for the geochemical surveillance of Mt. Etna, *Acta Vulcanol*., 4, 149-156, 1994.

Dzurisin D., Wicks C Jr, Tatcher W. 1999. Renewed uplift at the Yellowstone caldera measured by leveling surveys and satellite radar interferometry. Bull. Volcanol. 61, 349-355.

Ferrara, V., Idrogeologia del versante orientale dell'Etna, in: Proc.of the 3rd Intern. Conf. on Groundwaters, 91-144, 1975.

Ferrara V. & Pennisi A. (1993) – Elementi di valutazione del pericolo di inquinamento delle acque sotterranee da discariche di R.S.U. nell'area etnea. Atti 2° Conv. Int. di Geoidrologia, in Quaderni di Tecniche di Protezione Ambientale, 49: 513-524, Pitagora Ed. Bologna.

Ghisetti, F., and L. Vezzani, Thin-skinned deformations of the Western Sicily thrust belt and relationships with crustal shortening: mesostructural data on the Mt. Kumeta-Alcantara fault zone and related structures, *Boll. Soc. Geol. It., 103,* 129-157, 1984.

Giammanco, S., M. Valenza, S. Pignato, and G. Giammanco, Mg, Fe, Mn and V concentrations in the groundwaters of Mount Etna (Sicily), *Water Res*., 2, 378-386, 1996.

Giammanco, S., M. Ottaviani, M. Valenza, E. Veschetti, E. Principio, S. Giammanco, and S. Pignato, Major and trace elements geochemistry in the groudwaters of a volcanic area: Mount Etna (Sicily), *Wat. Res*., 32, 19-30, 1998a.

Gottsmann, J., R. Carniel, N. Coppo, L. Wooller, S. Hautmann and H. Rymer, H. (2007). Oscillations in hydrothermal systems as a source of periodic unrest at caldera volcanoes: Multiparameter insights from Nisyros, Greece, Geophys. Res. Lett., 34, L07307,doi:10.1029/2007GL029594.

Gudmundsson, A., S. S. Berg, K. B. Lyslo, and E. Skurtveit (2001), Fracture networks and fluid transport in active fault zones, J. Struct. Geol.,

23, 343–353.

Hirn, A., R. Nicolich, J. Gallart, M. Laigle, L. Cernobori, and ETNASEIS Scientific Group, Roots of Etna volcano in faults of great earthquakes, *Earth Planet. Sci. Lett*., 148, 171-191, 1997.

Hurwitz, S., and M. J. S. Johnston (2003), Groundwater level changes in a deep well in response to a magma intrusion event on Kilauea Volcano,
Hawai'i, Geophys. Res. Lett., 30(22), 2173, doi:10.1029/2003GL018676.

Joron, J. L., and M. Treuil, Etude géochimique et pétrogenèse des laves de l'Etna, Italie, *Bull. Volcanol*., 47, 1125-1144, 1984.

Koizumi, N., Y. Kitagawa, N. Matsumoto, M. Takahashi, T. Sato, O. Kamigaichi, and K. Nakamura (2004), Preseismic groundwater level
changes induced by crustal deformations related to earthquake swarms off the east coast of Izu Peninsula, Japan, Geophys. Res. Lett.,
31, L10606, doi:10.1029/2004GL019557.

Lentini, F., The geology of the Mt. Etna basement. Mem. Soc. Geol. It. 23, 1982, 7-25.

Liotta, M., D'Alessandro, W., Bellomo, S., Brusca, L., 2016. Volcanic plume fingerprint in the groundwater of a persistently degassing basaltic volcano: Mt. Etna. Chem. Geol. 433, 68-80. doi:10.1016/j.chemgeo.2016.03.032

Lo Giudice, E., G. Patanè, R. Rasà, and R. Romano, The structural framework of Mount Etna, *Mem. Soc. Geol. It.*, 2_3, 125-158, 1982.

Lowenstern J. B., Smith R. B., Hill D. P. Monitoring super-volcanoes: geophysical and geochemical signals at Yellowstone and other large caldera systems. Phil. Trans. R. Soc. A (2006) 364 , 2055–2072. doi:10.1098/rsta.2006.1813

Mattia M., Bruno V., Caltabiano T., Cannata A., Cannavò F., D'Alessandro W., Di Grazia G., Federico C., Giammanco S., La Spina A., Liuzzo M., Longo M., Monaco C., Patanè D., Salerno G., 2015. A comprehensive interpretative model of slow slip events on Mt. Etna's eastern flank. Geochem. Geophys. Geosyst., 16, doi:10.1002/2014GC005585.

Neri M., Casu F., Acocella V., Solaro G., Pepe S., Berardino P., Sansosti E., Caltabiano T., Lundgren P., Lanari R. (2009) Deformation and eruptions at Mt. Etna (Italy): A lesson from 15 years of observations Geophisical Research Letters, Vol. 36, L02309, doi:10.1029/2008GL036151, 2009

Newhall, C. G., S. E. Albano, N. Matsumoto, and T. Sandoval (2001), Roles of groundwater in volcanic unrest, J. Geol. Soc. Philipp., 56, 69–84.

Niwa M., Takeuchi R., Onoe H., Tsuyuguchi K., Asamori K., Umeda K., Sugihara K. (2012) Groundwater pressure changes in Central Japan induced by the 2011 off the Pacific coast of Tohoku Earthquake. *Geochem. Geophys. Geosyst.;*13:Q05020. doi:10.1029/2012gc004052.

Ogniben, L., Lineamenti idrogeologici dell'Etna, Rivista Mineraria Siciliana, 100-102, 1-24, 1966.

Oppenheimer C. Volcanic Degassing (2003) Treatise on Geochemistry ISBN (set): 0-08-043751-6 Volume 3; (ISBN: 0-08-044338-9); pp. 123–166

Paonita A., Caracausi A., Iacono-Marziano G., Martelli M., Rizzo A., 2012. Geochemical evidence for mixing between fluids exsolved at different depths in the magmatic system of Mt Etna (Italy), Geochim. Cosmochim. Acta, 84, 380–394.

Parello, F., D'Alessandro, W., Aiuppa, A., Federico, C., 2001. Cartografia geochimica degli acquiferi etnei. Gruppo Naz. per la Difesa dalle Catastrofi Idrogeologiche del C.N.R. — pubbl. n. 2190. Officine Grafiche Riunite, Palermo.

Patanè, D., Aiuppa, A., Aloisi, M., Behncke, B., Cannata, A., Coltelli, M., Di Grazia, G., Gambino, S., Gurrieri, S., Mattia, M., and Salerno, G., 2013. Insights into magma and fluid transfer at Mount Etna by a multiparametric approach: A model of the events leading to the 2011 eruptive cycle. Journal of Geophysical Research-Solid Earth 118, 3519-3539.

Rasà, R., F. Ferrucci, S. Gresta, and D. Patanè, Etna: sistema di alimentazione profondo, assetto geostatico locale e bimodalità di funzionamento del vulcano, in: Proc. of the National Conference on Progetto-Etna 1993-1995: Stato di avanzamento delle ricerche, pp. 145-150, Giardini Editori, Pisa, 1995.

Reid, M. E., 2004. Massive collapse of volcano edifices triggered by hydrothermal pressurization. Geology 32, 373–376.

Rizzo, A., A. Caracausi, R. Favara, M. Martelli, P. M. Nuccio, A. Paonita, A. Rosciglione, and M. Paternoster (2006), New insights into magma
dynamics during last two eruptions of Mount Etna as inferred by geochemical monitoring from 2002 to 2005, Geochem. Geophys. Geosyst.,
7, Q06008, doi:10.1029/2005GC001175.

Roeloffs, E. A., and A. T. Linde (2006), Borehole observations of continuous strain and fluid pressure, in Volcano Deformation: Geodetic Monitoring
Techniques, edited by D. Dzurisin, chap. 9, pp. 305–322, Springer, Chichester, U. K.

Rojstaczer, S.A., Ingebritsen, S.E., Hayba, D. O., 2008. Permeability of continental crust influenced by internal and external forcing. Geofluids 8, 128–139.

Romano, R., Succession of the volcanic activity in the Etnean area, *Mem. Soc. Geol. It*., 23, 27-48, 1982.

Schilirò, F., Proposta metodologica per una zonazione geologico tecnica del centro abitato di Maletto, *Geologia Tecnica*, 3/88, 32-53, 1988.

Shibata, T., and F. Akita (2001), Precursory changes in well water level prior to the March, 2000 eruption of Usu volcano, Japan, Geophys. Res.
Lett., 28, 1799–1802.

Tanguy, J. C., M. Condomines, and G. Kieffer, Evolution of the Mount Etna magma: Constraints on the present feeding system and eruptive mechanism, *J. Volcanol. Geotherm. Res*., 75, 221-250, 1997.

Thomas, M.E., Petford, N., Bromhead, E.N., 2004. The effect of internal gas pressurization on volcanic edifice stability: evolution towards a critical state. Terra Nova 16, 312–317.

Van Gaalen J.F., Kruse S., Lafrenz W.B., Burroughs S.M. Predicting Water Table Response to Rainfall Events, Central Florida (2013) Groundwater Vol. 51, No. 3 May-June 2013 (pages 350–362) doi: 10.1111/j.1745-6584.2012.00970.x

Ventura, G. and G. Vilardo (2005), Estimates of fluid pressure and tectonic stress in hydrothermal/volcanic areas: A methodological approach,
Ann. Geophys., 48(4–5), 797–803.

Voight, B., and D. Elsworth (2000), Instability and collapse of hazardous gas-pressurized lava domes, Geophys. Res. Lett., 27, 1–4.

Whitaker, S. (1986), Flow in porous media I: A theoretical derivation of Darcy's law, Transp. Porous Media, 1, 3–25.

Figure

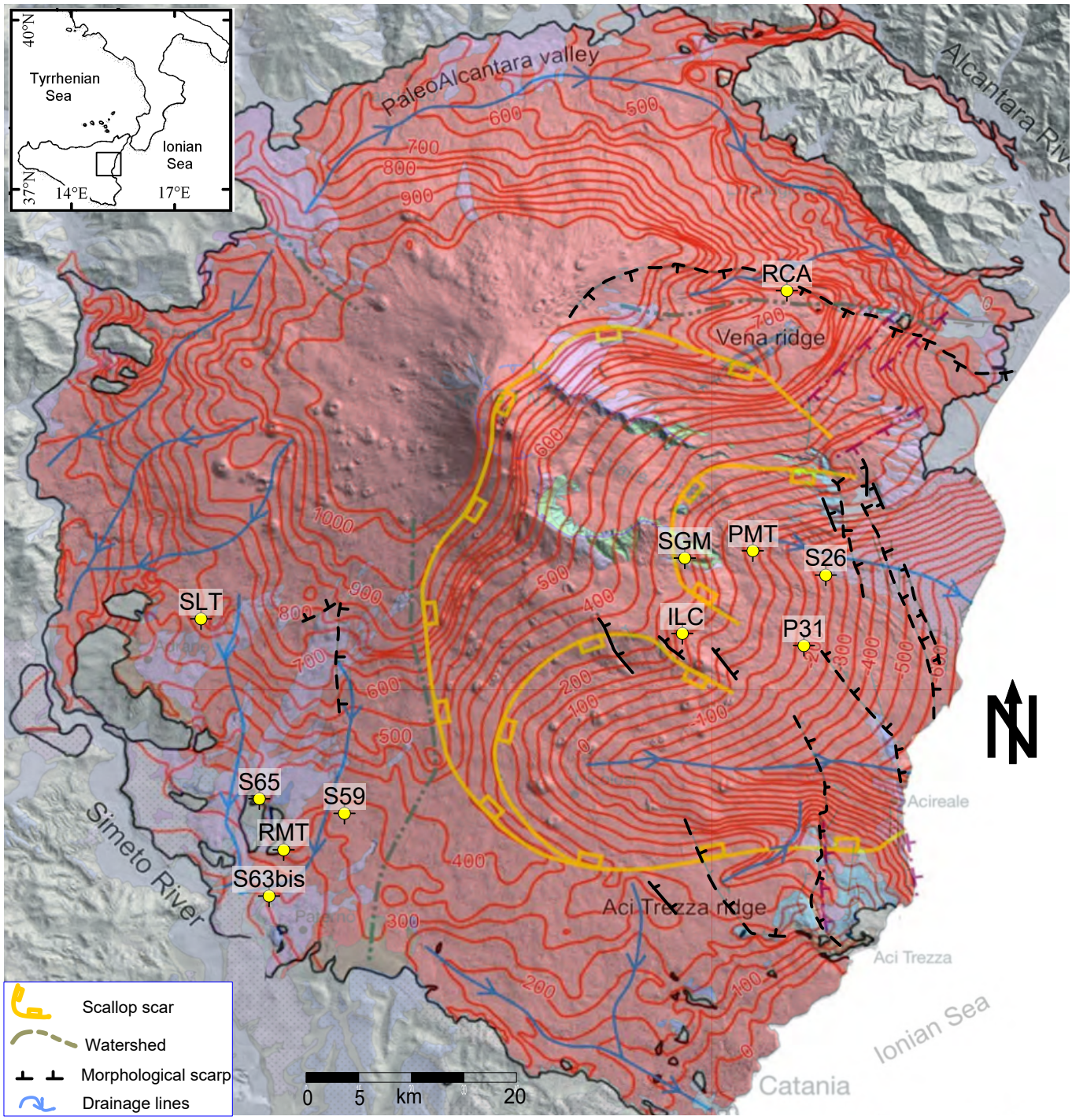
40°N
Tyrrhenian Sea
Ionian Sea
37°N
14°E
17°E
PaleoAlcantara valley
Alcantara River
RCA
Vena ridge
SGM
PMT
S26
ILC
P31
SLT
S65
S59
RMT
S63bis
Simeto River
Acireale
Aci Trezza ridge
Aci Trezza
Ionian Sea
Catania
Scallop scar
Watershed
Morphological scarp
Drainage lines
0 5 km 20

Figure

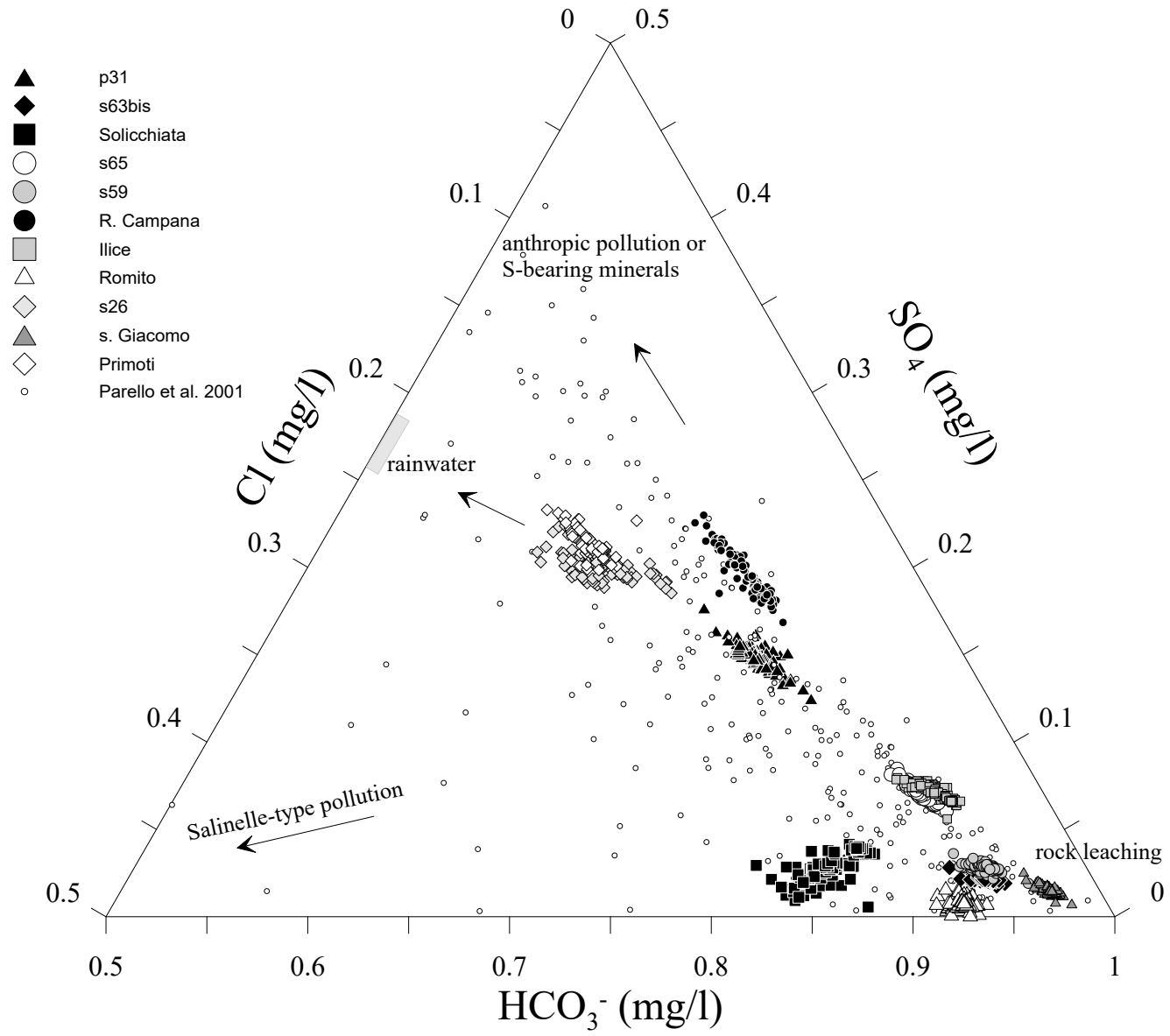

Figure 2

Figure

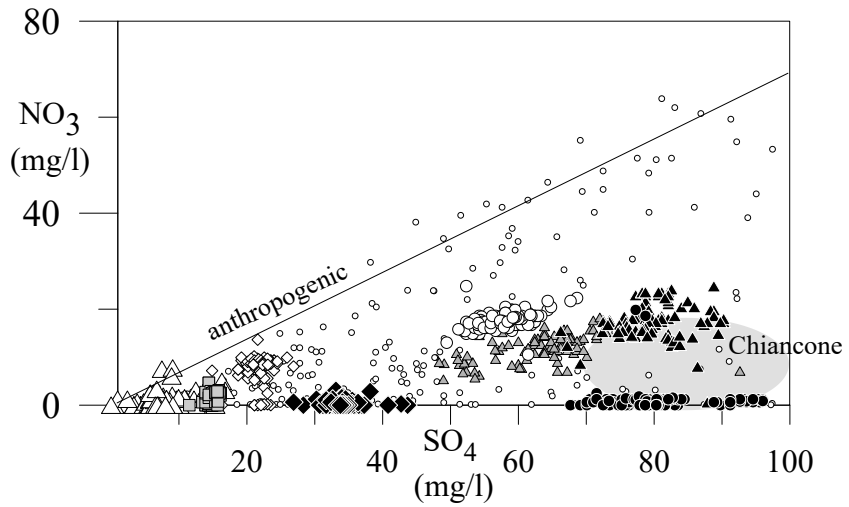

Figure 3

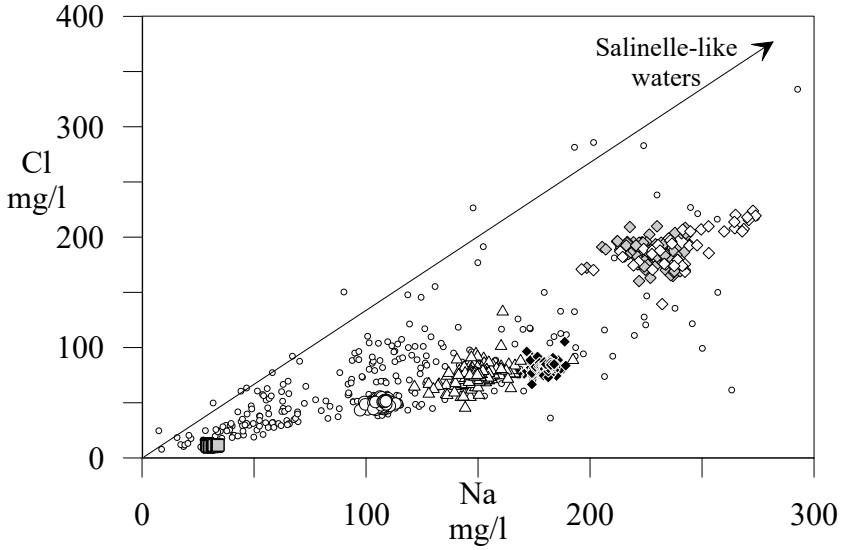

Figure 4

Figure

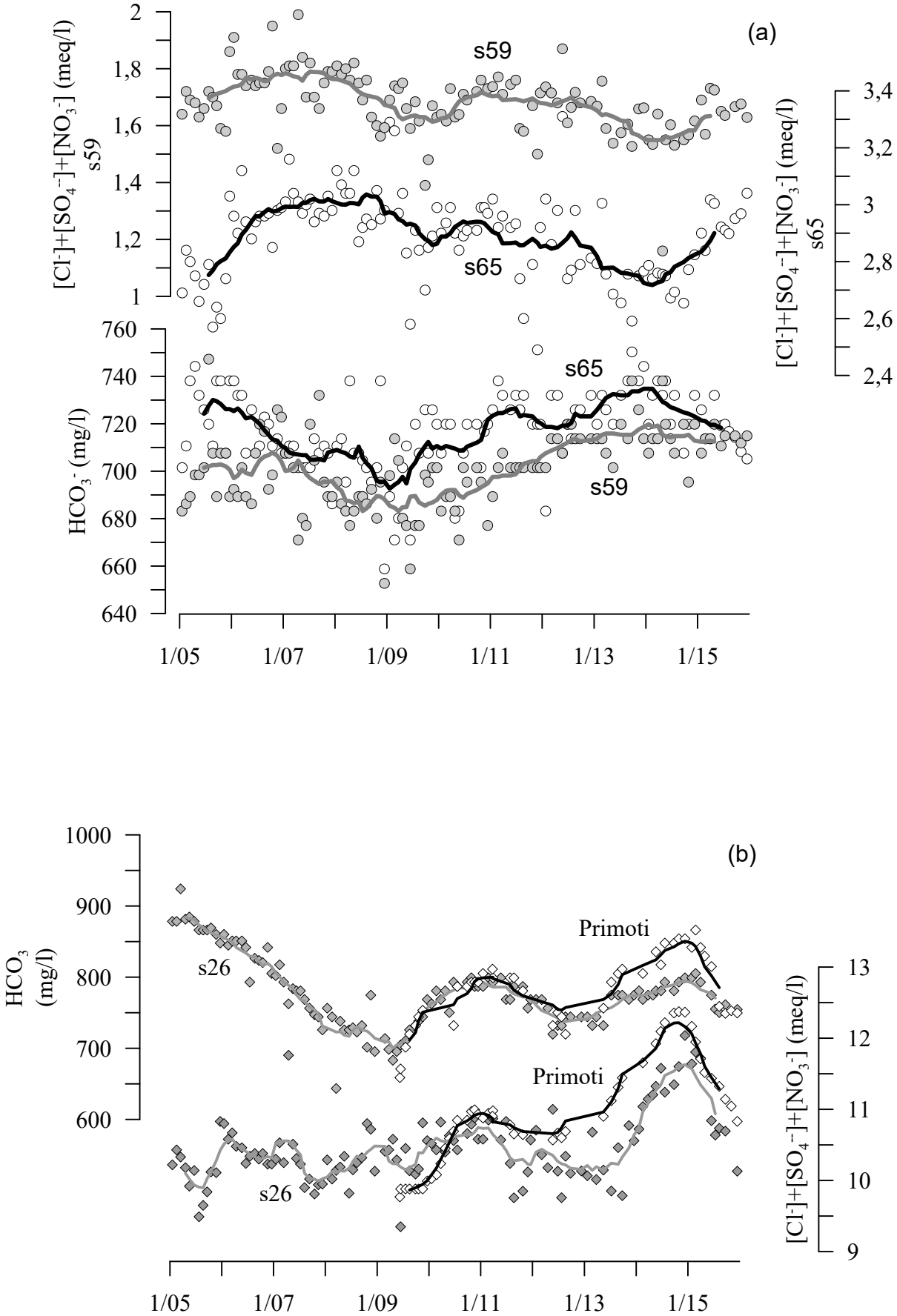

Figure 5

Figure

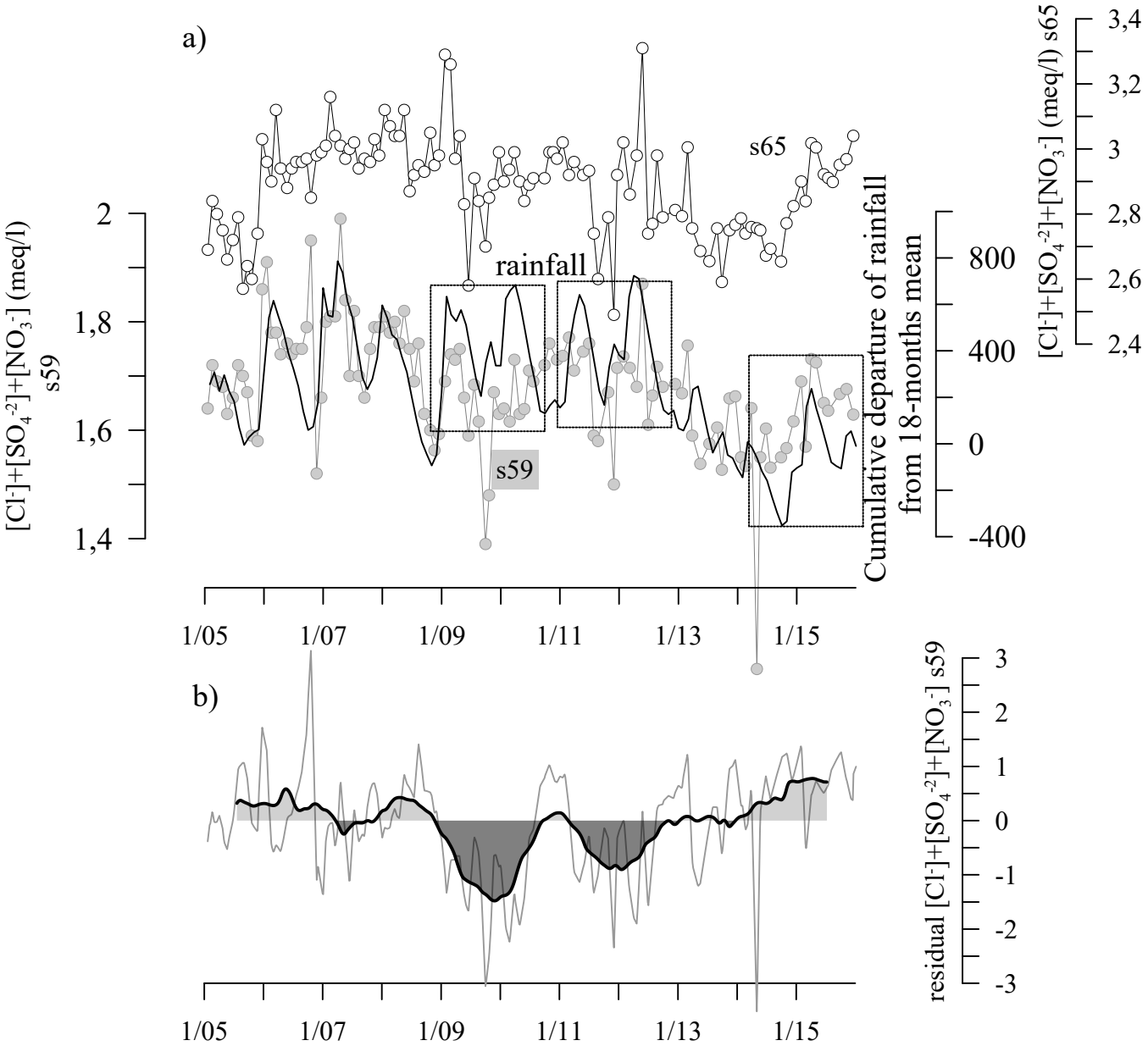

Figure 6

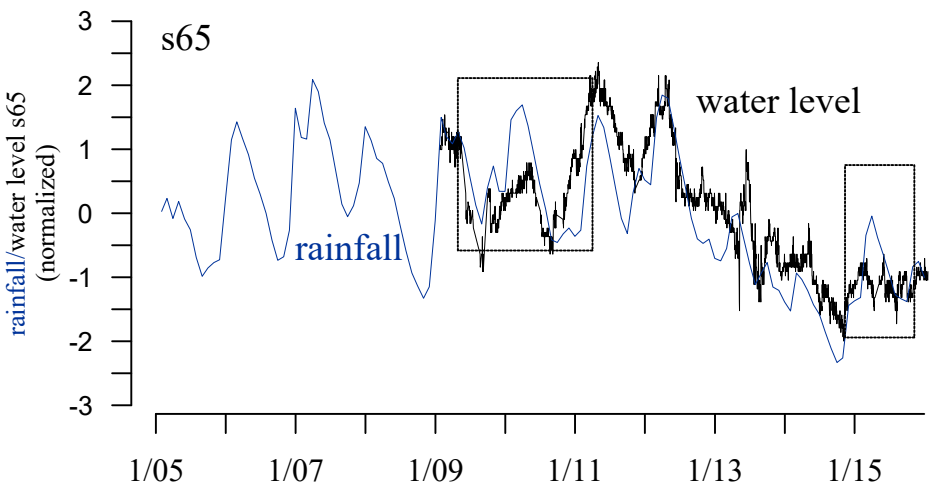

Figure 7

Figure

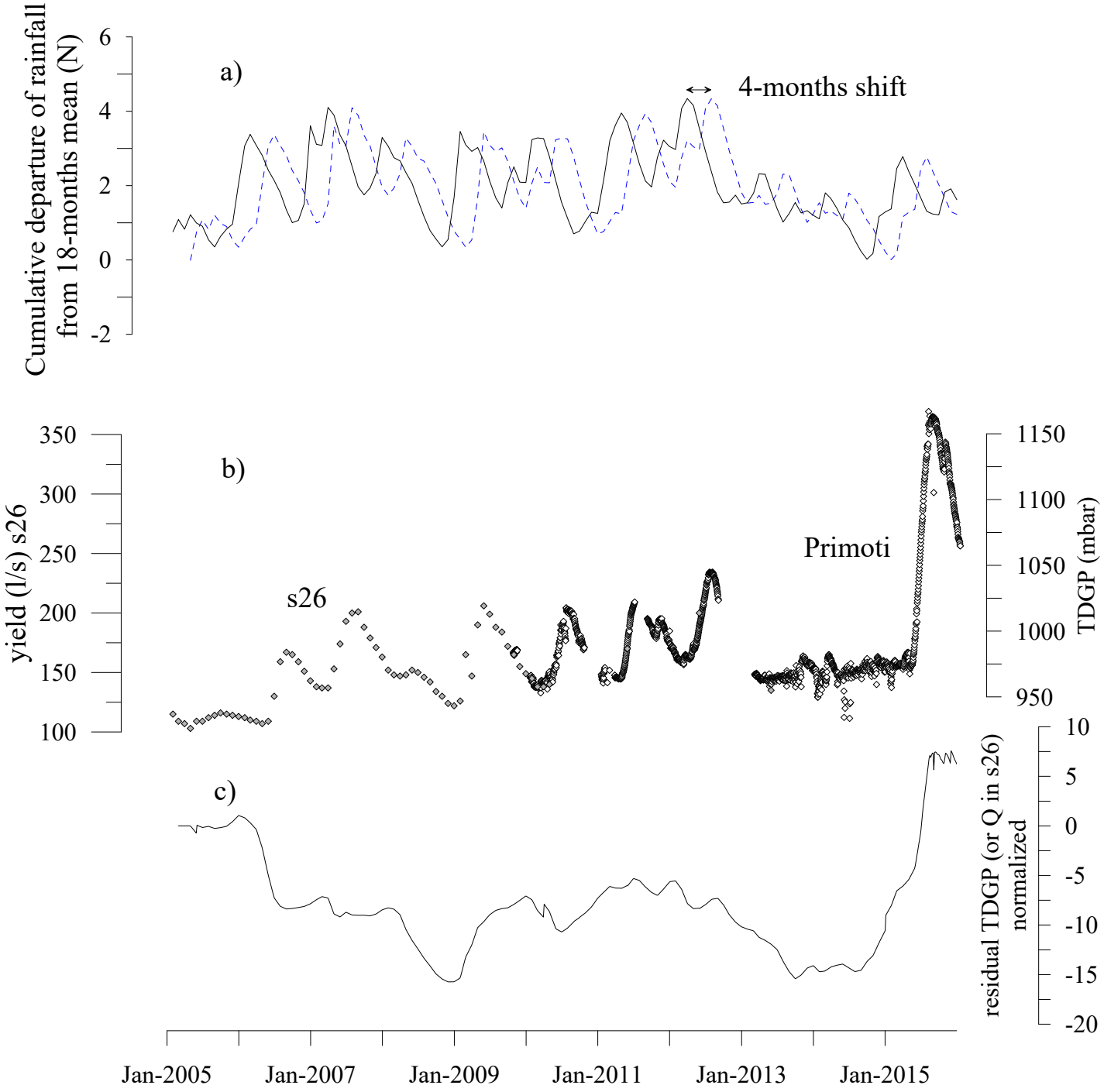

Figure 8

Figure

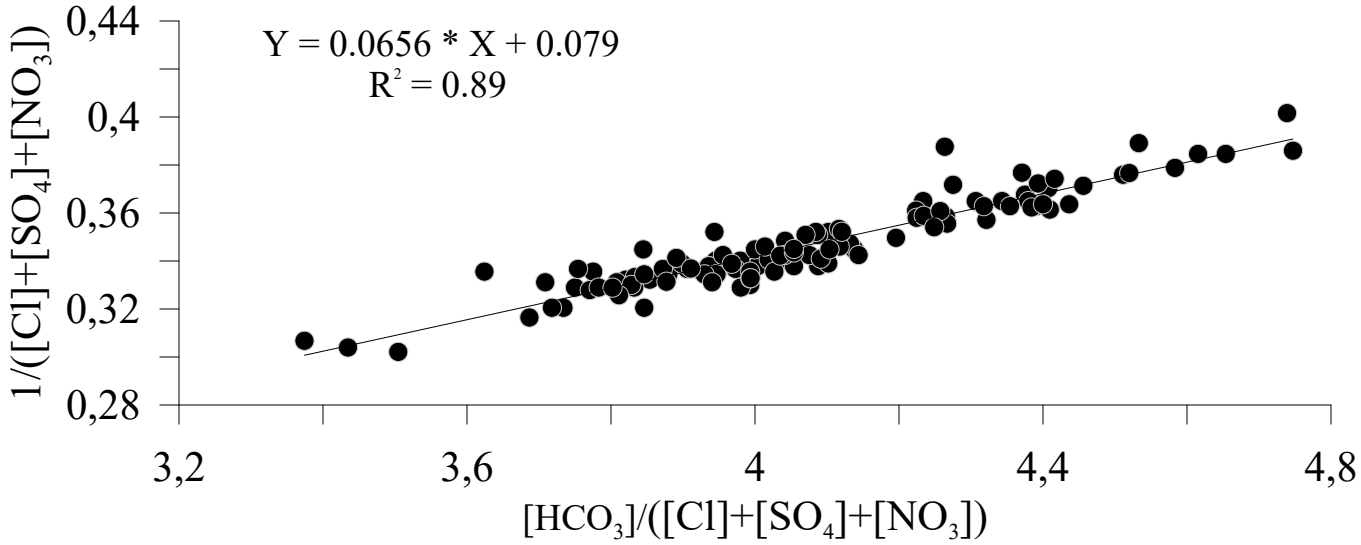

Figure 9

Figure

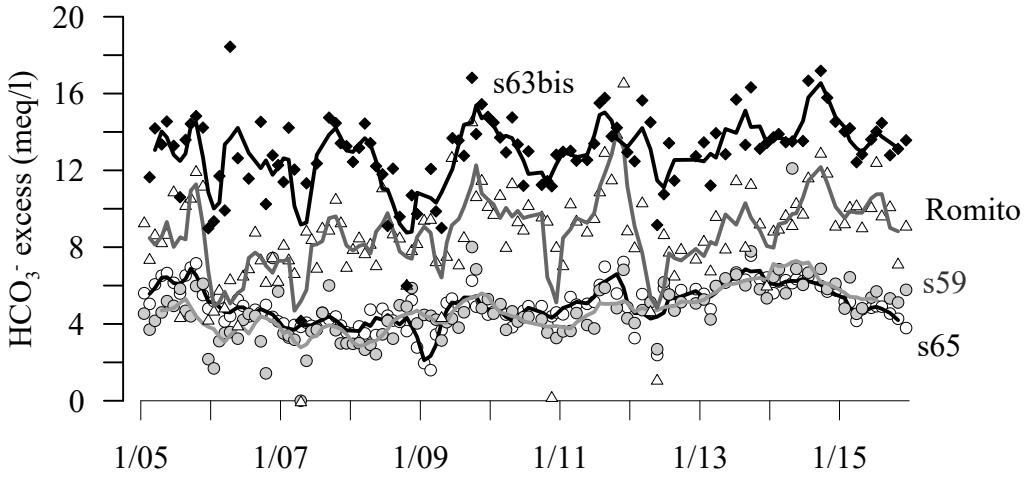

Figure 10

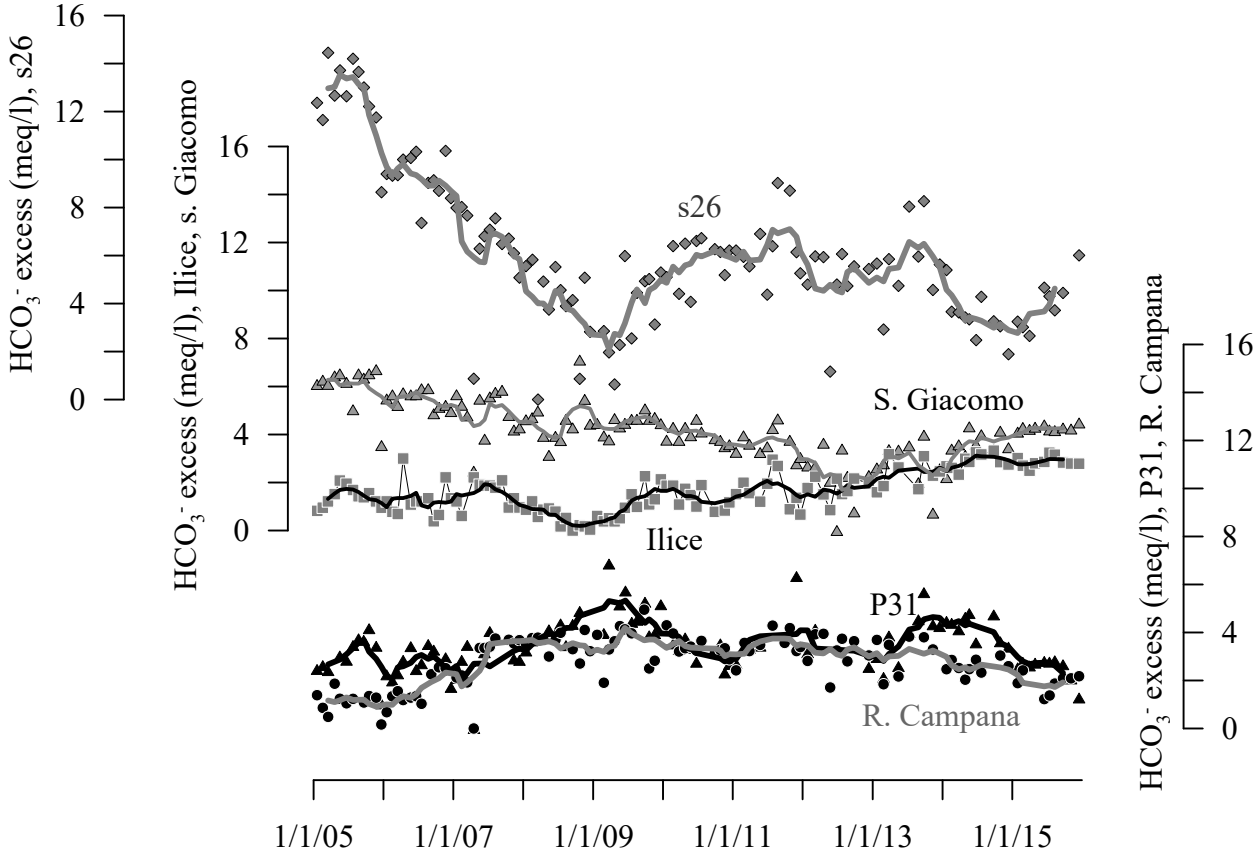

Figure 11

Figure

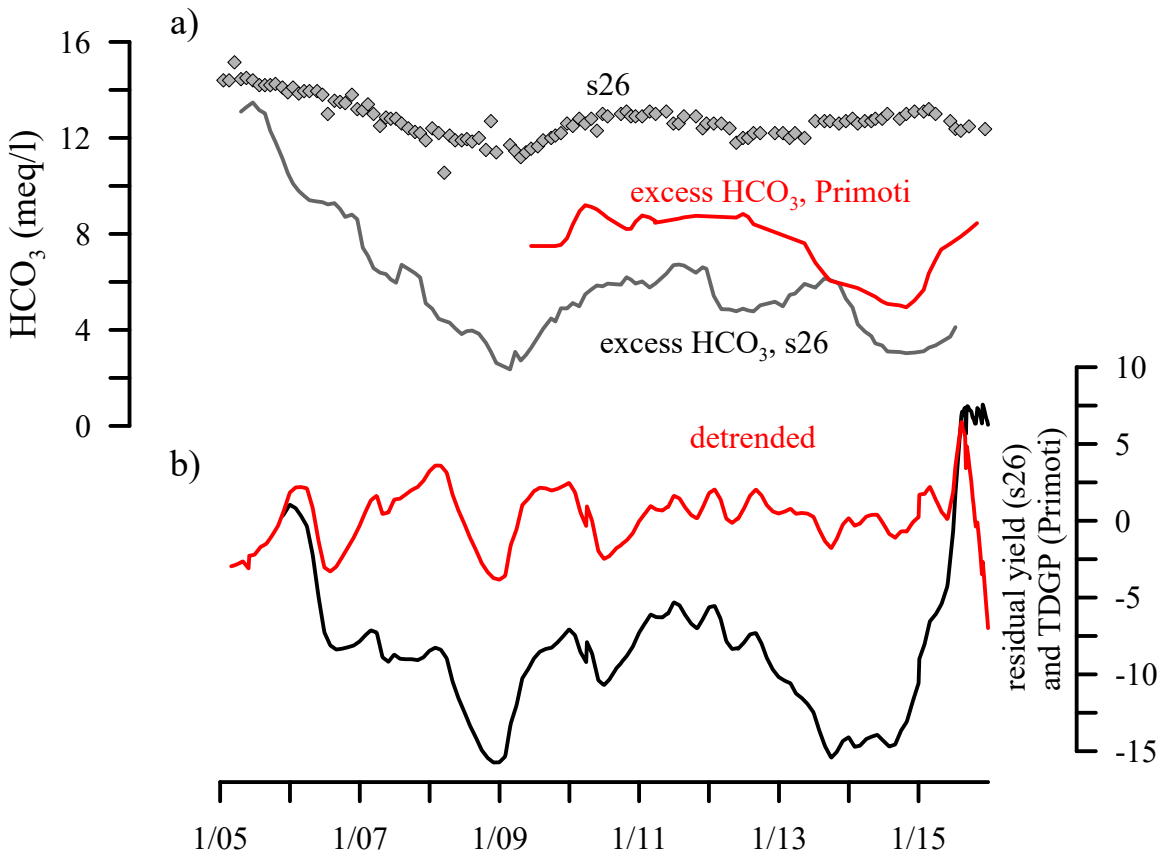

Figure 12

Figure

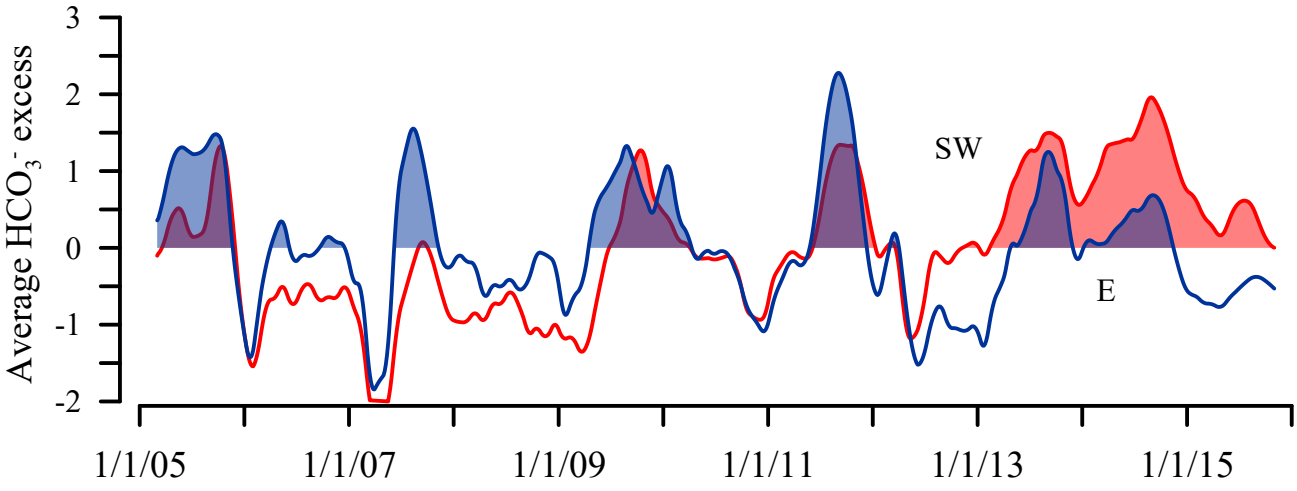

Figure13

Table

Click here to download Table: Tabella.doc

Sample name	Sample ID		Temp °C	pH	Na mg/l	K mg/l	Mg mg/l	Ca mg/l	F mg/l	Cl mg/l	NO_3 mg/l	SO_4 mg/l	HCO_3 mg/l	TDS mg/l
S65	[S65]	mediana	14.00	6.77	107.17	20.84	88.94	45.87	0.53	49.63	17.73	58.56	719.80	1107.66
		media	14.04	6.77	106.63	20.78	88.88	45.60	0.48	49.37	17.76	58.15	716.76	1104.35
		percentile 5%	13.89	6.68	101.91	19.55	84.18	41.26	0.30	44.67	15.49	52.32	683.20	1066.20
		percentile 95%	14.30	6.86	109.46	21.51	93.02	48.92	0.57	53.18	20.46	62.93	738.10	1133.10
S59	[S59]	mediana	14.70	6.24	104.88	19.16	70.24	49.06	0.57	39.00	8.68	21.73	701.50	1015.54
		media	14.86	6.25	104.38	19.10	70.22	48.85	0.56	39.11	7.78	21.75	701.28	1013.43
		percentile 5%	14.30	6.14	100.71	18.38	67.42	45.85	0.29	34.71	0.15	19.20	677.10	980.17
		percentile 95%	15.80	6.40	107.26	20.06	73.18	51.90	0.76	43.67	9.68	24.00	723.46	1039.29
Romito	[RMT]	mediana	15.50	6.75	149.88	19.64	110.25	53.51	0.57	77.64	0.00	6.72	997.35	1417.98
		media	15.46	6.76	150.22	19.70	110.26	53.33	0.66	77.92	0.79	6.87	994.64	1414.98
		percentile 5%	15.10	6.67	144.27	18.75	106.79	49.70	0.38	71.72	0.00	3.36	972.80	1386.53
		percentile 95%	15.70	6.88	155.27	20.82	114.22	55.71	0.76	85.47	3.10	12.48	1012.60	1438.88
S63Bis	[S63bis]	mediana	19.10	6.04	179.85	18.77	144.04	126.05	0.36	81.76	0.00	33.63	1416.73	2000.82
		media	19.12	6.04	179.29	18.34	144.09	125.83	0.33	82.01	0.21	33.87	1418.90	2003.57
		percentile 5%	18.60	5.95	172.27	15.64	139.26	120.71	0.07	75.15	0.00	30.94	1386.07	1962.98
		percentile 95%	19.70	6.12	185.16	19.55	150.98	129.46	0.55	89.72	1.24	37.14	1461.26	2057.72
Solicchiata	[SLT]	mediana	17.40	6.92	274.80	27.76	143.61	33.47	0.57	186.82	2.48	39.84	1220.00	1930.81
		media	17.44	6.93	277.71	27.72	144.56	33.38	0.72	187.48	2.15	39.42	1224.71	1938.94
		percentile 5%	17.07	6.80	244.75	25.81	132.44	29.60	0.26	141.47	0.00	19.54	1137.16	1782.04
		percentile 95%	17.70	7.07	315.15	28.93	158.36	36.87	0.76	244.27	4.83	52.74	1342.00	2131.54
P31	[P31]	mediana	15.60	6.08	80.38	21.11	46.05	44.89	0.38	55.30	17.36	79.63	402.60	745.43
		media	15.68	6.07	80.81	21.16	46.66	45.04	0.42	55.26	17.40	80.29	401.69	749.06
		percentile 5%	14.97	5.98	75.80	19.94	44.10	42.48	0.12	47.75	12.40	72.98	378.20	714.86
		percentile 95%	16.59	6.17	86.56	22.29	50.82	49.16	0.57	61.49	23.56	89.00	427.92	803.40
S26	[S26]	mediana	18.20	6.65	226.77	43.40	101.92	79.82	0.57	187.18	6.01	244.56	774.70	1670.18
		media	18.24	6.67	226.85	43.46	101.48	80.18	0.59	185.95	5.71	246.03	778.71	1669.86
		percentile 5%	16.95	6.50	213.77	41.02	93.65	72.85	0.30	168.92	2.54	221.04	703.79	1559.04
		percentile 95%	19.50	6.90	241.05	46.59	110.57	88.43	0.76	203.48	8.06	275.72	871.54	1786.85
Ilice	[ILC]	mediana	10.10	6.16	277.76	30.34	8.60	14.46	17.23	0.38	11.34	2.48	15.33	176.90
		media	10.15	6.16	284.62	30.91	8.65	14.87	17.79	0.36	11.24	2.19	15.03	183.45
		percentile 5%	9.70	6.04	262.73	29.08	8.21	13.33	16.23	0.24	10.28	0.00	13.92	167.75
		percentile 95%	10.70	6.28	321.49	33.62	9.43	17.78	20.33	0.43	12.41	3.10	15.84	211.67
San Giacomo	[SGM]	mediana	11.80	6.49	582.82	25.19	8.03	38.89	60.12	0.19	10.99	0.56	6.72	433.10
		media	11.78	6.50	593.25	25.87	8.06	39.92	61.12	0.21	10.99	0.48	6.91	439.59
		percentile 5%	11.40	6.35	541.01	23.82	7.43	35.79	55.51	0.00	9.57	0.00	6.24	396.50
		percentile 95%	12.11	6.63	658.56	26.82	8.60	44.83	69.14	0.29	12.79	1.06	8.28	494.10
Rocca Campana	[RCA]	mediana	12.90	7.07	81.50	13.29	33.66	16.37	0.35	34.74	0.80	78.72	298.90	558.81
		media	12.93	7.10	83.01	13.26	33.87	16.66	0.32	35.18	1.09	80.95	297.13	561.80
		percentile 5%	12.70	6.85	78.35	12.51	30.50	15.10	0.15	31.91	0.00	71.04	274.87	527.15
		percentile 95%	13.20	7.46	89.73	14.08	37.40	18.95	0.38	39.00	1.42	95.38	317.20	604.71
Primoti	[PMT]	mediana	18.70	6.27	239.08	44.18	104.23	78.30	0.61	192.14	4.34	261.60	793.00	1702.88
		media	18.83	6.25	241.32	44.33	103.19	79.16	0.91	191.43	3.50	265.34	782.30	1712.02
		percentile 5%	18.11	6.10	213.58	40.76	91.03	69.46	0.37	170.20	0.00	225.33	703.33	1543.34
		percentile 95%	19.68	6.35	270.81	47.68	114.89	87.54	0.95	219.29	6.79	315.51	853.39	1893.38

Supplementary Interactive Plot Data (CSV)

Click here to download Supplementary Interactive Plot Data (CSV): Supplemental material.csv